

1 **Review of pH sensing materials from macro- to nano-scale: recent**
2 **developments and examples of seawater applications**

3

4 Roberto Avolio^{*a}, Anita Grozdanov^b, Maurizio Avella^a, John Barton^c, Mariacristina Cocca^a,
5 Francesca De Falco^a, Aleksandar T. Dimitrov^b, Maria Emanuela Errico^a, Pablo Fanjul-
6 Bolado^d, Gennaro Gentile^a, Perica Paunovic^b, Alberto Ribotti^e, Paolo Magni^{*e,f}

7

8 ^a National Research Council of Italy, Institute for Polymers Composites and Biomaterials (CNR-IPCB),
9 Via Campi Flegrei 34, 80078 Pozzuoli (NA), Italy

10 ^b Faculty of Technology and Metallurgy, Ss. Cyril and Methodius University in Skopje, Skopje, North
11 Macedonia

12 ^c Tyndall National Institute, University College Cork, Lee Maltings Complex, Dyke Parade, Cork,
13 T12R5CP, Ireland

14 ^d Metrohm DropSens, Vivarium Ciencias de la Salud, C/Colegio Santo Domingo de Guzmán, 33010,
15 Oviedo, Spain

16 ^e National Research Council of Italy, Institute for the Study of Anthropogenic Impact and Sustainability
17 in Marine Environment (CNR-IAS), 09170 Oristano, Italy

18 ^f International Marine Centre (IMC), Loc. Sa Mardini, Torregrande, 09170, Oristano, Italy

19

20 *Corresponding authors: roberto.avolio@ipcb.cnr.it; paolo.magni@cnr.it

21

22 ORCID:

23 Roberto Avolio: <https://orcid.org/0000-0002-5733-0161>

24 John Barton <https://orcid.org/0000-0002-0671-5678>

25 Francesca De Falco: <https://orcid.org/0000-0003-3782-4540>

26 Pablo Fanjul-Bolado: <https://orcid.org/0000-0002-9224-1666>

27 Alberto Ribotti: <https://orcid.org/0000-0002-6709-1600>

28 Paolo Magni: <https://orcid.org/0000-0001-5955-6829>

29

30

31

Accepted Manuscript.

32

The final version is available at:

33 **[https://www.tandfonline.com/doi/full/10.1080/10643389.2020.1843312](https://www.tandfonline.com/doi/full/10.1080/10643389.2020.1843312?scroll=top&needAccess=true)**

34

2?scroll=top&needAccess=true

35

<https://doi.org/10.1080/10643389.2020.1843312>

36 **Abstract**

37 Over the last few decades, a large number of pH sensitive materials with new compositions and
38 structures have been proposed. Solid state sensors based on organic, inorganic and composite
39 materials are actively investigated, with an increasing interest in the performance offered by nano-
40 scale materials. Our review provides a thorough, up-to-date knowledge of a wide range of pH
41 measurement methods and related-sensing materials, firstly by introducing well established materials
42 and methods for pH sensing and then, by covering recent developments in inorganic, organic and
43 nano-engineered devices. The main sensor parameters, including sensitivity, stability, response time
44 and testing conditions are reported. Given the importance of pH sensing in environmental
45 applications, in particular seawater monitoring, sensors tested in seawater are highlighted and
46 discussed.

47

48

49 **Key words:** pH sensors; environmental monitoring; nanomaterials; water quality

50 **1. Introduction**

51 Due to the relevance of pH for many chemical and biochemical processes, pH measurements are
52 routinely carried out in a very broad range of activities, from industrial processes to chemical, medical,
53 and environmental monitoring.

54 pH strongly affects environmental and biological processes. The availability of nutrients, the uptake of
55 pollutants like heavy metals, the occurrence and distribution of microorganisms, the efficiency of
56 enzymatic bioprocesses and metabolism, the occurrence of oxidative stress and its consequences on
57 living organisms, are all pH-related phenomena (González Durán et al., 2018; Jin & Kirk, 2018; Kahn
58 et al., 2017). Accurate quantification of pH is then vital for monitoring the health of our planet. In
59 particular, pH is intimately linked with the dynamics of nutrients, contaminants, and trace metals in
60 seawater and is entangled with the complex ocean carbonate system. As the pH of ocean surface
61 decreases (-0.15 since pre-industrial times due to increasing dissolution of atmospheric CO₂, Clarke
62 et al., 2015), the delicate equilibria among chemical species in solution are perturbed, with effects on
63 coastal biodiversity (Gambi et al., 2016; Kurihara, 2008; Tagliapietra et al., 2012), and the functioning
64 (Lacoue-Labarthe et al., 2016) and health (Kroeker et al., 2013; Somero et al., 2016) of marine
65 ecosystems worldwide. Continuous, accurate and punctual recording of seawater pH is needed to
66 increase our understanding of the local and global pH dynamics and enable a better prediction of their
67 effects (Bushinsky et al., 2019; Stow et al., 2009).

68 Ion sensitive glass electrodes are the most popular pH sensors, due to their reliability, affordability
69 and fast (few s) response time. This includes environmental applications like seawater monitoring and
70 most oceanic probes are equipped with this kind of pH sensors for routine pH recording. However,
71 glass electrodes exhibit signal instability or drift and, therefore, require constant re-calibration: this
72 operation can cause significant errors, that may arise from the quality and handling of the calibration
73 solutions (McLaughlin et al., 2017b). The need for an inner electrolyte solution, connecting the
74 reference electrode with the sample solution through a liquid junction, can be another source of error
75 as the potential that develops across the junction varies as a consequence of external factors like
76 pressure. Finally, glass electrodes are brittle, need a storage solution and cannot be miniaturized.

77 For all these reasons, a number of alternative pH sensing devices have been proposed over the last
78 few decades. High precision measurements (up to 0.001 pH units) can be provided by
79 spectrophotometric devices that are, however, much more expensive and complex than
80 potentiometric sensors and have long sampling time (up to minutes). Solid state sensors can provide
81 a cheap, robust and miniaturizable alternative for pH measurements (Korostynska et al., 2007), as
82 demonstrated by the presence on the market of Ion Sensitive Field-Effect Transistors (ISFETs) based
83 pH probes. These features can be exploited to realize sensing system with low cost, low power
84 consumption and ease of operation (Radu et al., 2015). For the specific case of seawater pH, a
85 discussion of measurement problems and techniques can be found in specialized papers (Byrne,
86 2014; Marion et al., 2011); the quest for sensors with optimal field performance is still open (Okazaki
87 et al., 2017).

88 This review will discuss developments in the field of solid-state pH sensors, covering organic,
89 inorganic and composite sensing materials and focusing on recent devices based on nanomaterials.
90 Parameters like sensitivity, stability, robustness to interfering ions and response time of the sensors
91 will be reported and organized in tables for a fast reference. Recent examples of pH sensors
92 developed for seawater applications will be provided and reviewed at the end of each chapter.
93 Providing a thorough, up-to-date knowledge of a wide range of pH measurement methods and
94 related-sensing materials, our review may assist materials scientists, sensors developers and marine
95 scientists interested in new pH sensing solutions.

96

97 **2. Traditional methods and materials for pH measurement**

98 The hydrogen ion is a ubiquitous species that plays a role in most chemical and biochemical reactions
99 carried out in aqueous solutions. Firstly introduced by the Danish biochemist Soren Peter Lauritz
100 Sorensen, pH is defined as the negative logarithm of H⁺ activity (Sørensen, 1909; Buck et al., 2002):

$$101 \quad pH = -\log(a_{H^+}) \quad (1)$$

102 Due to the importance of this parameter for a wide range of applications, pH measurements are
103 routinely performed in chemical, industrial, biological and medical practice. In the following sections,
104 well established measurement techniques will be summarized, introducing some examples of
105 seawater-designed devices.

106 **2.1 Optical/spectrophotometric methods**

107 A practical measurement of pH can be obtained using the so-called acid-base indicators, substances
108 that change their color as a function of pH. In general, an indicator dye is an amphoteric compound
109 with a dissociation constant that is close to the pH to be determined. The pH of the sample-indicator
110 system can be expressed as a function of the dissociation constant of the indicator (pK) and of the
111 concentration of its protonated (HA) and unprotonated (A⁻) form:

$$112 \quad pH = pK + \log \frac{[A^-]}{[HA]} \quad (2)$$

113 As the two forms of the indicator in solution have different colors due to different light absorption, their
114 concentration can be measured from their absorption spectra.

115 Based on this principle, spectrophotometric methods for pH measurement, reaching an accuracy as
116 high as 0.001, have been developed using different indicators such as m-cresol purple, cresol red,
117 bromocresol green, bromocresol purple and thymol blue (King & Kester, 1989; Millero et al., 2009). A
118 schematic example of automated spectrophotometric pH system is reported in Figure 1. Once
119 calibrated, these devices do not need to be recalibrated for use at sea. A description of a
120 spectrophotometric pH sensor designed for in situ measurements can be found in Cullison Gray et al.
121 (2011) and in Lai et al. (2018).

122 Recent technological developments of optical/spectrophotometric-based sensors represent a
123 promising tool for monitoring the ocean carbonate system. In particular, pH sensors using

124 spectrophotometric techniques are currently used for surface water measurements on research
 125 vessels and, similarly, optodes for pCO₂ measurements have been successfully tested in seawater for
 126 oceanographic applications (Rérolle et al., 2018; Staudinger et al., 2018; 2019 and references
 127 therein). Optical methods for pH detection will not be further discussed. A comprehensive review can
 128 be found in (Rérolle et al., 2012).

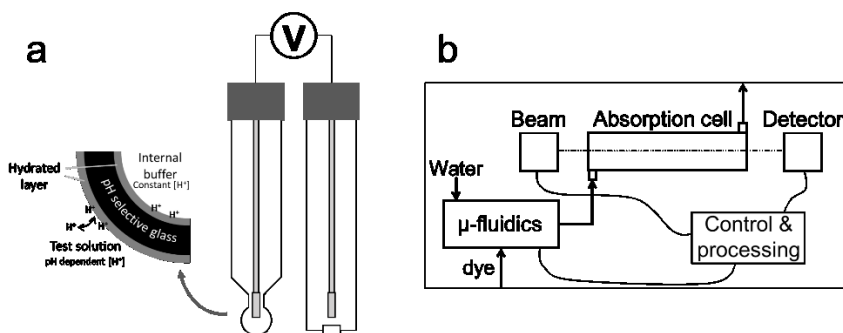
129 2.2 Electrochemical methods

130 Probably the most common techniques for pH sensing are based on the measurement of electrical
 131 parameters, such as conductivity or resistivity, impedance, potential. Conductometric devices
 132 correlate the change in conductivity/resistivity of an active material connecting two electrodes to the
 133 concentration of the analyte (H⁺ for pH). Voltammetric devices measure the current flowing between
 134 the electrodes when the potential is swept in a defined manner; in this case, the pH measurement can
 135 be correlated to a peak potential of an electroactive compound (Dai et al., 2016).

136 Potentiometric sensors are the most used for routine pH determination. In principle, a potentiometric
 137 measurement consists of the measurement of the electromotive force (EMF) in an electrochemical
 138 cell, composed of a working electrode and a reference electrode. The pH of the sample is calculated
 139 comparing the EMF measured in the sample (E_s) and in a standard buffer solution (E_b) of known pH
 140 (pH_b), following the Nernst equation:

$$141 \quad pH = pH_b + \frac{(E_b - E_s)F}{RT \ln 10} \quad (3)$$

142 where R is the gas constant, F is the Faraday constant and T is the temperature (Rérolle et al., 2012).



143
 144 **Figure 1.** Scheme of: a potentiometric pH sensor with glass ion sensitive electrode (a) and a spectrophotometric
 145 pH measurement device (b).

146 The most used working electrode for this application is made of a silver/silver chloride electrode
 147 embedded into a glass tube that ends in an ion selective glass membrane. On both sides of the glass
 148 membrane, a hydrated gel layer is formed with the aqueous solutions that are in contact with glass
 149 surfaces (Figure 1). The concentration of H⁺ ions on the inner layer, containing a reference solution, is
 150 constant while on the outer layer it varies depending on pH. As a consequence, there is an exchange
 151 of alkaline ions between the outer layer and the glass membrane that changes the overall potential of
 152 the membrane. The reference electrode is usually of the same type (Ag/AgCl), immersed into a KCl
 153 solution and can be included with the working electrode in a single device.

154 The glass electrode potentiometric equipment is relatively cheap and has been the only practical way
155 to measure pH of seawater for many years. However, the glass electrodes must be handled with care
156 due to the brittleness that is associated with glass, and properly stored in electrolyte solutions to
157 prevent ions leaching from the glass membrane (if stored in deionized water) and to preserve the
158 hydrated layer onto glass surface from drying out. They also have a limited shelf life due to the
159 degradation of the glass membrane and need a regular calibration in seawater buffers, whose
160 accurate preparation determines the accuracy of the measurement (McLaughlin et al., 2017b;
161 Weldborg et al., 2009). The stability and pressure sensitivity of the “liquid junction”, the porous
162 membrane that allows an ion flow to close the electrochemical cell, can also be an issue. In practice,
163 electrode potential drift and experimental problems can limit the accuracy of potentiometric
164 measurements to less than 0.01, with a drift of 0.02 pH/day (R  rolle et al., 2012).

165

166 **3. Inorganic materials for solid state sensors**

167 The realization of a miniaturizable, stable and cheap pH sensor to substitute glass membrane based
168 devices is still a challenge. A number of solid-state sensors have been proposed and some of them
169 are already available on the market.

170 A common approach to solid state Nernstian pH sensors is based on the realization of Ion Sensitive
171 Field Effect Transistors (ISFETs). ISFETs are traditional Metal Oxide Semiconductor Field Effect
172 Transistors (MOSFET), where the gate electrode is modified (or substituted) by a thin layer of an
173 insulating material (Si_3N_4 , Al_2O_3 , Y_2O_3 , ZrO_2). The protonation/deprotonation process occurring on the
174 insulator layer when in contact with water solutions of different pH determines the electrostatic field at
175 the gate, controlling the current flowing into the FET (Bergveld, 2003). The circuit must be closed
176 using a reference electrode connected to the source in lieu of the now removed gate (liquid gating).

177 ISFET pH sensors exploit a mature (more than 20 years) technology and have been used extensively
178 for industrial, clinical and environmental pH monitoring as they offer a number of advantages, relative
179 to glass electrodes. First, the sensor can be fabricated with conventional silicon based semiconductor
180 technologies at reduced costs and ease of integration with electronic devices. Furthermore, it is small,
181 resistant to mechanical shock and does not need a storage solution. Due to the different structure, the
182 impedance of ISFET devices is lower with respect to glass electrodes, which has a beneficial effect
183 on noise and stability. Commercially available sensors based on ISFET technology have been tested
184 at sea with encouraging results and devices specifically designed for oceanographic research, mainly
185 based on the Honeywell Durafet™ sensor, are currently used by research institutions (Johnson et al.,
186 2016; Saba et al., 2019).

187 Despite the good performance of ISFET sensors, further refinements are required for their extended
188 use in ocean acidification studies, concerning, as an example, the reliability of the reference
189 electrode, long signal stabilization time and the stability of the sensor during long-term oceanic
190 deployments (Martz et al., 2015; McLaughlin et al., 2017a; R  rolle et al., 2012).

191 A wide number of variations to the standard ISFET design have been proposed over the years. Some
 192 examples of the most advanced solutions will be reported here (see Table 1 for main parameters). A
 193 double gate architecture that can push sensitivity above the Nernst limit has been developed. As an
 194 example, a double gate ISFET based on ZnO was claimed, with a sensitivity as high as 2.25 V/pH
 195 (Spijkman et al., 2011a). The high sensitivity is generated by a capacitive coupling effect (Spijkman et
 196 al., 2011b) that, in this case, was maximized by applying an extremely thin passivation layer, a self
 197 assembled monolayer of octadecyl phosphonic acid. However, the device was tested only at the pH
 198 values of 6 and 8, and showed a large standard deviation in the measured potential. An alternative
 199 design to reduce noise and increase stability relies on the realization of an extended sensing layer,
 200 connected to the gate (extended-gate FET or EGFET; Pullano et al., 2018). Parizi et al. (2012)
 201 proposed a device that couples two EGFETs (n- and p- type) in parallel, matched to have the same
 202 transconductance to cancel a large part of the noise. This design allows the substitution of the
 203 external reference electrode (e.g. Ag/AgCl) with a simple, solid state pseudo-reference.

204 In a recent paper, Takechi et al. (2015) demonstrated a signal amplification effect similar to Spijkman
 205 et al. (2011a) using an amorphous InGaZnO₄ (IGZO) layer as the bottom gate and a thin film of TaO_x
 206 as an ion sensitive top gate. The resulting sensitivity is as high as 450 mV/pH but the resolution limit,
 207 calculated taking into account drift and hysteresis of the device, was estimated in 0.02 pH in a narrow
 208 range (pH 4 – 6). An optimization of the fabrication process led to a similar IGZO/Ta₂O₅ based ISFET
 209 with a sensitivity of 402 mV/pH in the 4 – 9 pH range (Kumar et al., 2017). However, stability and drift
 210 problems still constitute a serious limit to the use of this kind of device in demanding applications (Pyo
 211 & Cho, 2017). Ta₂O₅ has been investigated also for the realization of flexible extended gate
 212 electrodes, printed on plastics and coupled to a FET device (Wu et al., 2017). The sensitivity of this
 213 assembly was relatively low, 24 mV/pH, but good temporal stability (drift < 1% during tests) and
 214 repeatability were observed.

215 Recently, an interesting combination of organic semiconductor and SiO_x thin layer was tested as gate
 216 in a dual-gate ISFET device, showing an improvement in response time and an amplification of the
 217 signal up to 10 times with respect to a bare SiO_x layer (Pfattner et al., 2019). However, the stability of
 218 the response was not addressed.

219 In summary, ISFET devices take advantage of well-established semiconductor fabrication processes
 220 for the production and integration of pH sensors. It is a technology with a long history and a high
 221 maturity level, with at least one product dedicated to seawater application already on the market. In
 222 the quest for increased stability and accuracy, a number of improved designs have been proposed
 223 and tested at laboratory scale. Latest developments make use of nano-engineered active layers and
 224 electrodes and will be discussed in Section 5.

225 **Table 1.** Main characteristics of ISFET based sensors.

Sensing material and setup	Testing range and media	Sensitivity	Stability	Response time	Reference
ZnO Dual gate ISFET	6 – 8 Commercial buffers	Up to 2.25 V/pH	Low hysteresis. High standard deviation on	n/a	Spijkman et al., 2011a

			sensitivity estimation		
Al ₂ O ₃ EGFET	4 – 10	Up to 130 mV/pH	n/a	n/a	Parizi et al., 2012
TaO _x Dual gate ISFET	4 – 6 McIlvaine buffer (Na ₂ HPO ₄ – citric acid)	453 mV/pH Resolution up to 0.02 pH	Drift and hysteresis low with respect to the high response	n/a	Takechi et al., 2015
Ta ₂ O ₅ Dual gate ISFET	4 – 9 Commercial pH buffers	402 mV/pH	Relatively stable after 1.5 years of storage	n/a	Kumar et al., 2017
Ta ₂ O ₅ EGFET	1 – 13 Water + HCl/NaOH Weak effect of monovalent cations	28 mV/pH	<1% drift over 16 min	<10 s	Wu et al., 2017
SiO _x ISFET	2.4 – 11.7 PBS Response is not linear below pH 5. Low effect of varying NaCl concentration	Up to 14%/pH (drain current normalized to the reference value at pH 7.4)	n/a	Few s	Pfattner et al., 2019

226

227 A second family of solid state probes for pH are electrodes based on oxides or metal/metal oxide
228 couples, suitable for a potentiometric sensing setup. Metal/metal oxide pH sensors respond to pH due
229 to an equilibrium involving the metal and its oxide where, in the metal oxide electrodes, the metal is
230 not involved in the potential-determining reaction (Glab et al., 1989).

231 Due to their robustness, relatively easy miniaturization, fast response and good sensing performance,
232 metal/metal oxide and metal oxide materials represent promising substitutes to glass electrodes. pH
233 responsiveness has been observed in many semiconducting oxides, including Sb₂O₃, PtO₂, OsO₂,
234 Ta₂O₅, TiO₂, PdO, SnO₂, ZrO₂, PbO₂ and, notably, IrO₂ and RuO₂ (Hayat & Marty, 2014; Koncki &
235 Mascini, 1997; Yao et al., 2001).

236 Antimony based electrodes have been among the first to be developed and proposed (Kinoshita et
237 al., 1986). As the potential developed by antimony, in response to hydrogen ion activity, is to some
238 degree sensitive to other dissolved anions, the use of a Nafion membrane to cover the electrode has
239 been proposed, resulting in a response stable within 2 mV/pH over 1 month (Xu et al., 2016, 2018,
240 see Table 2).

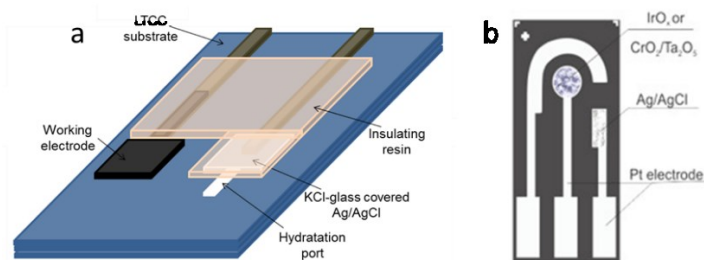
241 Ruthenium oxide is one of the most investigated oxides for pH sensors; its sensing mechanism is
242 attributed to the presence of oxygen vacancies at the surface that lead to the formation of hydroxyl
243 groups by dissociative adsorption of water, generating a pH sensitive layer (Trasatti, 1991). Thick
244 films can be produced by screen printing and 3D structures can be built by the low temperature co-
245 firing of ceramics (LTCC), both industrially scalable processes, showing very high sensitivity and
246 robustness (Figure 2; Manjakkal et al., 2014, 2016). Thick films based on RuO₂ containing glass paste
247 were fabricated by screen printing and sintering; potential was measured against Ag/AgCl in the pH
248 range 2-12 and a linear Nernstian behaviour was observed with a slope of 56 mV/pH. In a formulation
249 with 30 wt% of titania, the sensitivity was maintained at 56.11 mV/pH with a response time of about

250 15 s and a 60 days stability. In a similar way, mixed RuO₂/Ta₂O₅ based films were prepared by screen
251 printing and sintering with glass forming oxides. In this case, the response was higher in acidic to
252 neutral environment (64.7 mV/pH from 2 to 8) than in basic conditions (43.1 mV/pH from 8 to 11)
253 probably due to the effect of alkaline pH on the supporting glass paste (Manjakkal et al., 2016).
254 Remarkably, in these examples the behaviour of RuO₂ based sensors was not influenced by common
255 anions. However, an influence of oxygen and redox agents has been observed in industrial
256 applications of RuO₂ based sensors. Recently, a double protective layer (Ta₂O₅ thin film and Nafion
257 membrane) has been introduced to mitigate the effect of interfering species (Lonsdale et al., 2018).

258 Some of the reported papers, in the quest for miniaturization and integration of their sensors, propose
259 an integrated solid Ag/AgCl pseudo-reference electrode, to be fabricated into the same substrate as
260 the sensing electrode. The need for a stable reference is, in fact, a key problem for the development
261 of miniaturized solid pH sensors (Hu et al., 2015; Michalska, 2012). We can affirm that a robust and
262 stable alternative to liquid or gel filled electrodes is not yet available, although a number of different
263 designs for disposable and/or reusable solid pseudo-reference electrodes are available (Sophocleous
264 & Atkinson, 2017). The use of modern fabrication technologies can lead to miniaturized multilayered
265 electrodes with stability comparable to traditional ones (Moya et al., 2019).

266 Iridium oxide is also widely employed for pH sensing. It is usually indicated as IrO_x due to its complex
267 stoichiometry, strongly influenced by synthesis conditions (Jang & Lee, 2020). An optimized
268 electrodeposition, followed by an annealing procedure, was developed for the deposition of porous
269 IrO_x films onto gold electrodes (Kim & Yang, 2014). The modified electrodes (Figure 2) showed a
270 nearly perfect Nernstian response to pH changes, with a slope of 59 mV/pH very stable towards cyclic
271 pH changes. Iridium and tantalum oxide thin films were deposited onto platinum electrodes by means
272 of electro-deposition and e-beam sputtering respectively (Uria et al., 2016). Being designed for
273 biological media, these devices were tested in a phosphate buffer saline solution (PBS) within a
274 narrow pH range, resulting in a potentiometric response of 59.4 mV/pH for tantalum and 72 mV/pH for
275 iridium oxide.

276 IrO_x based sensors have good pH sensing performance but their response can be affected by
277 reactions with oxidizing and reducing species dissolved in the test solution. A tantalum oxide layer
278 deposited over IrO_x has been tested as a barrier layer, increasing the stability of the signal against
279 oxygen (Kuo et al., 2014). Recently, a further refinement in the oxidation procedure of iridium wires
280 led to the production of a remarkably stable sensor, with no need for barrier layers (Pan et al., 2018).
281 This sensor was tested in the presence of a large set of anions and cations and in marine water,
282 exhibiting stability and sensing performance in line with the glass electrode used as a reference. A
283 very similar Ir/Ir(OH)_x pH electrode has been recently fabricated and field tested in seawater,
284 comparing the results with a commercial pH meter (Zhang et al., 2017). The solid state electrode
285 showed good stability (137 days) and a precision comparable to the reference glass sensor, with a life
286 span up to 5 months.



287
 288 **Figure 2.** Assembly of: sintered RuO₂ working electrode onto LTCC ceramic substrate (a) (Reprinted from
 289 Manjakkal et al. (2016), with permission from Elsevier); gold electrode modified by electrodeposited IrO_x (b)
 290 (Reprinted from Uria et al. (2016), with permission from Elsevier). Both solutions include a pseudo-reference solid
 291 Ag/AgCl electrode.

292 Other metal oxides used for pH measurements include WO₃, TiO₂, ErO₂ and MnO₂. Manganese oxide
 293 was shown to exhibit a non-linear electrical response to pH (and a tendency to dissolve in acidic
 294 solutions) due to the chemical equilibrium among the oxide and the oxo-hydroxide species. A
 295 microelectrode was fabricated by coating MnO₂ with a polymeric proton-conductive Nafion membrane,
 296 showing a linear response in the 4 – 12 pH range with a slope of 60 mV/pH (Cachet-Vivier et al.,
 297 2010). In a recent study, a tungsten bronze with a well-defined composition and crystal structure was
 298 produced by oxidation of tungsten wire and has been proposed as electrode material for
 299 potentiometric pH detection (Cisternas et al., 2017). The response of this material was found to be
 300 highly reproducible and stable (variations in the order of 0.3 mV) upon storage and continuous
 301 operation conditions. The use of multiple metals in a single device has been investigated by Sadig et
 302 al. (2018) that realized an iridium, ruthenium and titanium oxide based tri-oxide system. Though no
 303 details are given on the structure of the deposited oxide layer, the response recorded showed a linear
 304 potential/pH relation whose slope was stable within 0.3 mV/pH over 120 days of testing. Finally, it is
 305 worth reporting on the design of a sensor based on solid metal rods, expressly developed for
 306 seawater monitoring (Brooke et al., 2016). To overcome the interferences of corrosion, surface
 307 reactions and fouling, 8 different metals were simultaneously used and their potential against a
 308 common zinc counter electrode was recorded continuously against pH, measured by a reference pH
 309 meter, allowing the calibration of the device through a self-learning neural network algorithm. After
 310 calibration, the device was able to reproduce actual pH values over 3 weeks of deployment.

311 **Table 2.** Main characteristics of metal/metal oxide based sensors. In bold, sensors that have been tested in
 312 seawater.

Sensing material and setup	Testing range and media	Sensitivity	Stability	Response time	Reference
Sb ₂ O ₃ – Nafion membrane Potentiometric	4 – 9 Commercial buffers	54.5 ± 2 mV/pH	Stable within 2 mV/pH over 1 month (measurement repeated every week)	20 s	Xu et al., 2018
RuO ₂ /TiO ₂ Potentiometric	2 – 12 HCl/NaOH solutions. Interference of Li ⁺ , Na ⁺ and K ⁺ negligible	56.11 mV/pH	Storage in ambient condition up to 2 months with no change in properties	15 s	Manjakkal et al., 2014

RuO ₂ /Ta ₂ O ₅ Potentiometric	2 – 12 HCl/NaOH solutions and H ₃ BO ₃ /citric acid/Na ₃ PO ₄ buffer. Interference of Li ⁺ , Na ⁺ and K ⁺ negligible	64.7 mV/pH (pH 2–8) 43.1 mV/pH (pH 8–11)	Storage in ambient conditions up to 2 months led to a small reduction in sensitivity	15 s	Manjakkal et al., 2016
IrO _x Potentiometric	2.4 – 11.6 Commercial buffers	59.5 mV/pH	n/a	2 s	Kim & Yang, 2014
Ta ₂ O ₅ / IrO _x Potentiometric	3 – 8 PBS acidified with HNO ₃ Chloride ion concentration can influence reference stability	59.4 mV/pH (Ta ₂ O ₅) 72 mV/pH (IrO _x)	Stable after incubation in LB/ glucose for 24 h	Few s	Uria et al., 2016
IrO _x Potentiometric	2 – 13 Britton – Robinson buffer Good selectivity against common cations	59.5 mV/pH	Drift < 0.1 mV/h	n/a	Kuo et al., 2014
Ir(OH) _x carbonate oxidized Potentiometric	2 – 10 Commercial buffers Tested in seawater (pH 7.9) Negligible effect of common cations anions and O ₂	56.8 – 57.6 mV/pH	No drift over 48 h at pH 6	1 s	Pan et al., 2018
Ir(OH) _x Potentiometric	4 – 9 Calibrated in commercial buffers Tested in Dickinson seawater (pH 7.876) and in open sea	56.1 – 59.5 mV/pH	Negligible drift over 200 s. Stable during 137 d of continuous recalibration in standard buffers	5 s	Zhang et al., 2017
MnO ₂ – Nafion membrane Potentiometric	2 – 12 H ₂ SO ₄ /NaOH solutions Interference by Fe ²⁺ ions	≈ 60 mV/pH	n/a	35 to 74 s	Cachet- Vivier et al., 2010
Na _{0.75} WO ₃ Potentiometric	1 – 10 Commercial buffers, KCl/HCl solution (pH 1) High selectivity against Na ⁺ K ⁺ Mg ²⁺ Ca ²⁺	≈ 56 mV/pH	Stable for storage in air up to 6 months and for repeated measurements over 1 w	13 – 18 s (depending on pH)	Cisternas et al., 2015; Cisternas et al., 2017
IrO ₂ -RuO ₂ -TiO ₂ Potentiometric	1 – 13 Tris buffer Some influence of K ⁺ ions	59 mV/pH	Stable within 0.3 mV/pH for 120 d	4 – 8 s	Sadig et al., 2018
Stainless Steel, Cu, WC, Brass, Ni, Al, Ti, Bronze Potentiometric vs a common Zn counter- electrode	Tested in seawater	Neural network calibration correlates potential readings with pH	Signal degradation after 1 month of deployment	n/a	Brooke et al., 2016

313

314 Some of the studies presented have tested the use of metal oxide pH sensors in seawater. Zhang et
315 al. (2017) integrated four IrO_x pH electrodes and one Ag/AgCl reference electrode in a self-made
316 chemical sensor, and deployed it in a profile detection of nearly 70 m for a sea trial, near Newport

317 Harbor, California. The pH value measured by the sensor was very close to the data given by a Sea-
318 Bird 911 plus CTD, taken as a reference (maximum deviation 0.06 pH units), with the IrO_x sensor
319 showing a better data matching in the 0–40 m water depth range. The sensors were subjected to
320 periodic calibrations for a 137 days period, showing a remarkable response stability. The authors
321 contend that the high precision and accuracy of the sensor make it possible to use in the ocean
322 observation field.

323 Pan et al. (2018), fabricated an IrO_x based electrode, whose response to pH was tested in various
324 buffers and in seawater samples. Their sensors showed a good agreement (maximum deviation 0.04
325 pH units) with a commercial glass electrode in all testing conditions, showing a negligible interference
326 of other dissolved ions. No data is available for long term deployment in seawater.

327 Furthermore, Brooke et al. (2016) described the simultaneous use of eight metal electrochemical cell
328 for measuring ocean pH through a non-linear calibration algorithm obtained using a neural network
329 self-learning approach. A prototype sensor was deployed in a seawater tank at the Seattle Aquarium
330 for one month and, after the calibration period, was able to reproduce pH values within 0.02 pH units
331 vs. the reference pH electrode for up to 3 weeks, before corrosion and fouling started to affect the
332 response.

333 The latest developments in the field of inorganic films, for both FET and potentiometric pH sensing
334 devices, are directed towards the fabrication of nanostructured/multilayer electrodes with improved
335 performance and reduced cost. These approaches will be treated in Section 5.

336

337 **4. Polymer-based pH sensors**

338 Polymer based materials, in particular conducting polymers, are finding ever increasing applications in
339 the sensing field, due to their versatility, low cost and robustness (Adhikari & Majumdar, 2004).

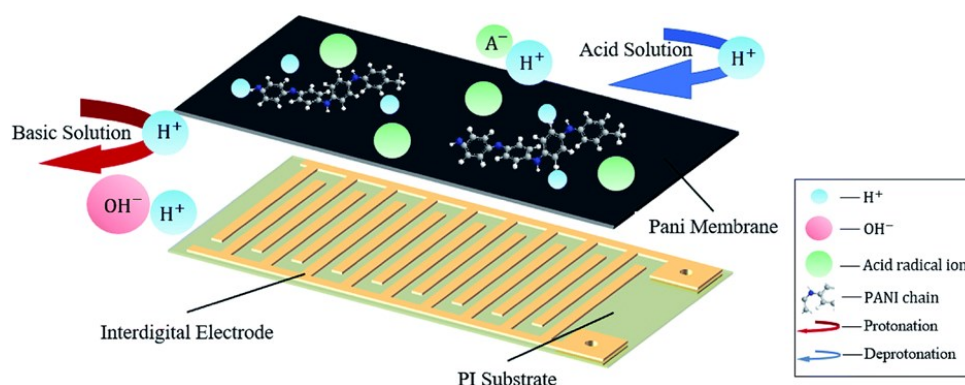
340 A general feature of conducting polymers is their “redox” activity and, as a consequence, the
341 possibility to change their electrical behaviour (charge carrier density, band structure) through a
342 doping-dedoping effect generated by the interaction with ions or small molecules (Adhikari &
343 Majumdar, 2004; Culebras et al., 2014). These interactions constitute the basis for the use of
344 conducting polymers for sensing (Gupta et al., 2004; Persaud & Pelosi, 1985).

345 Huang et al. (1986) investigated in detail the effect of pH on conducting polymers, in particular
346 polyaniline (PANI) and showed that the pH influences the redox processes of PANI in aqueous
347 electrolytes. Since the first pioneering studies, the most investigated polymers in sensing have been
348 polythiophene, polypyrrole (Ppy) and, notably, polyaniline and its derivatives, deposited or
349 polymerized directly onto metal electrodes.

350 Doped PANI can be produced by electrochemical polymerization of aniline in the presence of
351 tetraphenyl borate (Pandey & Singh, 2001). The potentiometric measurement carried out in buffers
352 and electrolytic solutions showed a linear potential/pH relationship, and a claimed stability of 6 months
353 (Table 3). However, a super-Nernstian response was observed, attributed to a non equilibrium
354 protonation/deprotonation process. In a more complex design, a graphite lead was covered with in

355 situ polymerized PANI (Gao & Song, 2009) and used for amperometric sensing of pH in the range 1.8
 356 – 9.9. The voltammetric current/potential curve shifted towards negative potential with increasing pH,
 357 showing a bilinear correlation and high reproducibility (0.5% error on repeated measurements). The
 358 higher slope recorded in the acidic range was attributed to multiple oxidation states possible for PANI.
 359 Recently, disposable and low cost sensors were realized by drop casting a PANI solution on carbon
 360 electrodes, printed on a paper substrate. Ag/AgCl solid pseudo-references were produced on the
 361 same substrate to fabricate an integrated device that showed a linear response to pH in the range 4 –
 362 10, stable during 24 h (Rahimi et al., 2016). Flexible interdigitated electrodes deposited on a
 363 polyimide film (Figure 3) have been covered by spin casting with a PANI film, doped with dodecyl
 364 benzene sulfonic acid (Li et al., 2020). The flexible sensors were calibrated in phosphate buffers and
 365 showed a linear potential response vs. pH up to pH 8.6.

366 Platinum electrodes, realized by photolithography, have been modified with polypyrrole and used by
 367 Lakard et al. (2007); the potentiometric response of these sensors was tested in the pH range 2 – 11,
 368 showing a nearly linear dependence of potential with pH. The sensitivity, however, showed a
 369 progressive decrease over 30 days of monitoring, attributed to the degradation of the silver pseudo-
 370 reference electrode. Ppy polymerized onto PEI modified electrodes showed improved stability, due to
 371 the adhesion granted by the imine layer (Segut et al., 2007). As a more recent example of a
 372 potentiometric sensor made by electropolymerization, it is worth mentioning the device proposed by Li
 373 et al. (2011). By polymerization of bisphenol A (BPA) onto indium tin oxide (ITO) coated glass, the
 374 authors developed an electrode that was tested in either potentiostatic or potentiometric setup, in a
 375 wide pH range (1 to 14) showing a sensitivity close to the Nernst limit and a reasonable stability of the
 376 response up to 12 days.



377
 378 **Figure 3.** Schematic representation of an interdigitated gold electrode with deposited PANI sensing layer
 379 undergoing reversible protonation/deprotonation. Reproduced from Li et al. (2020) - Published by The Royal
 380 Society of Chemistry.

381 Recently, a non-conjugated, redox active polymer, poly(dopamine), demonstrated a linear correlation
 382 of the redox peak measured by voltammetry with pH. The polymer was deposited on a carbon
 383 electrode and tested in a wide pH range, in different buffers or saline solutions showing an excellent
 384 stability of the response (Amiri et al., 2016).

385 Combinations of conducting polymers with support polymers have been also realized by various
 386 methods, including the deposition of preformed polymer from solutions, reducing the cost of the
 387 assembly and overcoming the difficulties of electrodeposition. Gill et al. (2008) developed a composite
 388 conductimetric pH sensor mixing doped PANI particles with polyvinyl butyral and polypyrrole. The
 389 composite was deposited by screen printing on an interdigitated electrode and showed a linear
 390 response to pH in the range 2 – 8, but a response time of about 200 s. An analysis of the sensor
 391 response as a function of composition revealed that PANI is the active component while polypyrrole
 392 contributes to increase the system conductivity. As a development of this concept, a gel with similar
 393 composition was tested for the real time detection of pH in drinking water (Banna et al., 2014). Gold
 394 interdigitated electrodes were covered with the sensitive polymers and exposed to solutions in the pH
 395 range 6.5 – 9 showing a non-linear change in resistivity that was stable over 30 days of continuous
 396 exposure. The accuracy and resolution of these sensors were similar to commercial devices.

397 **Table 3.** Main characteristics of polymer based sensors.

Sensing material and setup	Testing range and media	Sensitivity	Stability	Response time	Ref.
PANI/ tetraphenylborate Potentiometric	2 – 9 Tris-HCl buffer Negligible effect of Na ⁺ , K ⁺ , Ca ²⁺	≈ 86 mV/pH	Stable after 6 months storage	n/a	Pandey & Singh, 2001
PANI Amperometric	1.8 – 9.9 Britton-Robinson buffer	32.4 mA/pH (pH 1.8 – 5.5) 15.9 mA/pH (pH 5.5 – 9.9)	0.5% error on consecutive measurements	5 s (85% of reading)	Gao & Song, 2009
PANI Potentiometric	4 – 10 Commercial buffers	50 mV/pH	Drift ≤ 0.01 pH/h during 24 h	12 s	Rahimi et al., 2016
PANI Potentiometric	5.45 – 8.62 Phosphate buffer	58.6 mV/pH 2.4% standard deviation	Hysteresis < 12% of full scale	54 s	Li et al., 2020
PEI / Ppy Potentiometric	4 – 9 Commercial buffers. Interference of carbonate ions	≈ 50 mV/pH Dependent on film structure	Slight decrease of sensitivity over 30 d	< 60 s	Segut et al., 2007
Poly(bisphenol A) Potentiostatic/ Potentiometric	-1 – 15 50nM NaCl + HCl or NaOH. No effect of Na ⁺ , K ⁺ , Cl ⁻ , SO ₄ ⁻	58.6 ± 1.4 mV/pH (Potentiostatic) 56.7 ± 1.6 mV/pH (Potentiometric)	Stable within ≈ 4% after 12 d of storage	20 s	Li et al., 2011
Poly(dopamine) Potentiostatic	1 – 12 Phosphate, acetate, carbonate, Britton-Robinson buffers. HCl/KCl solution	58.2 mV/pH	Stable within 0.8% for repeated measurement. Slight effect of buffer ionic strength, corrected by calibration	n/a	Amiri et al., 2016
PANI/ Ppy in poly(vinyl butyral) gel Conductometric	6.4 – 9 Tap water	Non-linear resistivity/pH calibration curve	Precision 0.07 pH units. Stable for 30 d of continued use	n/a	Banna et al., 2014

398

399 Polymer based pH sensors, mainly based on organic conductive polymers, have been known for a
 400 long time. Many different designs and compositions have been proposed, but their development has
 401 been limited up to now to lab scale studies. This fact can be due to the low compatibility of polymer

402 processing conditions with the traditional electronic technologies that rely on inorganic
403 semiconductors and oxides. Moreover, the relatively low stability of polymer electrical response may
404 have contributed to the low diffusion of polymeric sensors for pH monitoring. Nevertheless, the
405 popularity of polymer based sensors is now increasing, following the development of flexible, printable
406 organic electronics, and polymers can be the ideal candidates for the fabrication of disposable
407 devices with short service life. In the most recent research, conductive polymers are combined with
408 nanomaterials for enhanced sensitivity, response time and selectivity (Ates, 2013).

409

410 **5. Nanomaterial-based sensors**

411 The continuous quest for high sensitivity, fast response time, flexibility and cost-effectiveness is the
412 driving force for the research of new solutions and materials for sensing. The use of nanoscale
413 materials, both organic and inorganic in the realization of sensing devices, has been recently
414 proposed leading to very interesting improvements in sensor performance (Salavagione et al., 2014).

415 The first and more obvious consequence of the structuring at very small length scale, is the large
416 increase in surface area. As the interactions with probe solutions are usually limited to the surface of
417 the sensing material, this leads to an immediate increase in sensitivity that allows the design of
418 miniaturized devices with weight, energy and cost savings.

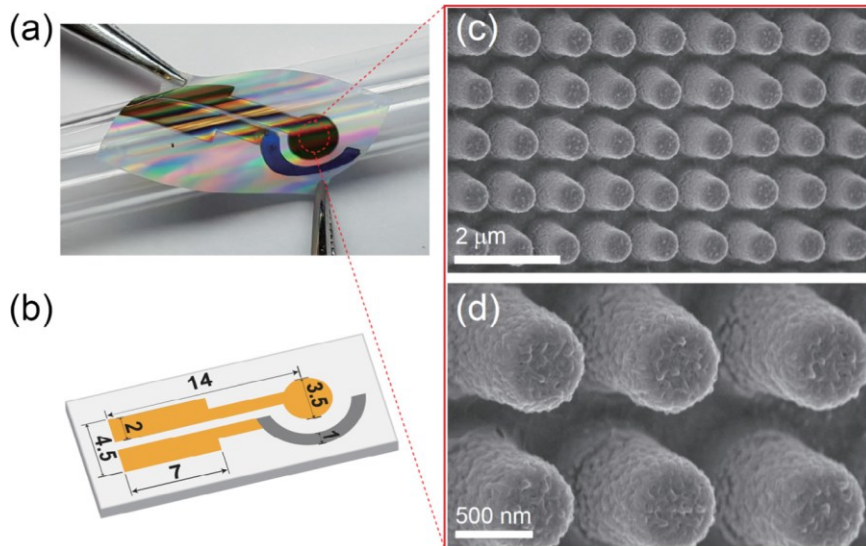
419 **5.1 Organic and carbon-based nanomaterials**

420 One-dimensional nanomaterials based on conducting polymers can be fabricated using well-
421 established wet chemical techniques and their properties can be easily tuned during synthesis or with
422 a doping step. Nanotubes and nanowires with enhanced sensitivity toward various chemical/biological
423 species are then ideal candidates for the design of new sensors (Bangar et al., 2010).

424 Nanowires fabricated with different methods have been proposed for the realization of pH sensing
425 devices. Shirale et al. (2010) fabricated a FET sensor based on a single PPy nanowire for real-time
426 pH monitoring and examined how the diameter of the nanowire affects the sensor performance. The
427 sensor showed a linear correlation of the drain current with pH in the range 1 – 11 (Table 4). Doped
428 Ppy nanowires were fabricated by electropolymerization on a gold substrate (Sulka et al., 2013). The
429 gold/Ppy electrode was then used as a potentiometric sensor in buffer solutions, in the pH range 2 –
430 12: it was shown that the oxidizing agent used for the polymerization influences the response, with
431 LiClO_4 giving the best sensitivity (49.3 mV/pH). Remarkably, the nanowires showed a ten-fold
432 increase in sensitivity compared with thin films of Ppy prepared in the same conditions.

433 Recent developments in polymer based pH sensors are generally directed towards the realization of
434 flexible devices, as an example, by printing carbon based electrodes onto plastic films and modifying
435 them with active materials. PANI nanofibers directly polymerized at the surface of carbon electrodes
436 supported on PET were tested at pH between 4 and 10 (Park et al., 2019). The Nernstian response
437 was observed with good repeatability (97.9%) and reasonable stability (drift of 3 mV/h over 15 h). An
438 interesting flexible pH sensor was fabricated by soft-lithography templating of nanopillars on a

439 polyurethane/acrylate layer followed by electrodeposition of polyaniline (Figure 4). A solid Ag/AgCl
440 pseudo-reference electrode was deposited as a reference and the sensor was tested in the 2 – 12 pH
441 range, showing a remarkably fast (≈ 1 s) and accurate response (compared to a reference glass
442 electrode) even in complex samples like juices and coffee (Yoon et al., 2017).



443
444 **Figure 4.** Templated nanopillars realized by soft lithography and flexible electrode assembly. Reprinted from
445 Yoon et al. (2017), with permission from Elsevier.

446 Dodecyl benzene sulfonic acid doped PANI nanoparticles were conveniently incorporated into an
447 epoxy resin to produce thin films for conductometric measurement of pH in soil (Patil et al., 2019).
448 The films showed a high conductivity when loaded with 10 wt% of PANI and were tested in
449 commercial buffers showing a linear response of relative conductance vs. pH.

450 Carbon nanotubes (CNTs) and graphene (G) are among the most investigated nanomaterials for
451 sensing applications, thanks to their unique chemical structure, very high conductivity, chemical
452 stability and high surface area (Chen et al., 2011; Martin & Escarpa, 2014).

453 Ideal graphene (G) is a single layer of sp^2 carbons arranged in a hexagonal structure extended in 2
454 dimensions (Li et al., 2009; Novoselov et al., 2012). Carbon nanotubes are tubular structures ideally
455 formed by rolling up one (single-wall, SWCNT) or more (multi-wall, MWCNT) graphene sheets. The
456 surface chemistry of carbon nanostructures can be tuned by the introduction of specific chemical
457 groups, influencing their electronic and chemical behaviour (Ramanathan et al., 2008; Tasis et al.,
458 2006). Graphene derived materials known as graphene oxide (GO) and reduced graphene oxide
459 (rGO) are interesting alternatives to graphene, showing higher reactivity at the expense of
460 conductivity.

461 An interesting report on the correlation of CNT conductivity with pH was published in (Lei et al., 2012).
462 The authors simply deposited a layer of multiwall CNTs onto filter paper and then showed a nice
463 correlation of the system resistivity with pH of buffer solutions. Similarly, the pH response of graphene
464 was observed on a simple resistive device, by deposition of exfoliated graphene onto a silicon wafer.
465 Platinum electrodes were then deposited and the resistivity measured showed a linear correlation with
466 pH, that was explained by an n- and p-doping effect induced by H^+ and OH^- ions respectively (Lei et

467 al., 2011). A number of studies show that the electrical response of graphene and CNTs exposed to
468 aqueous electrolyte solutions depend on various interfering factors (pH, dissolved ions, substrate
469 surface; Heller et al., 2010) and that the formation of charges at CNT or graphene surfaces is mainly
470 driven by the presence of “defects” (Back & Shim, 2006), such as oxidized groups (Tan et al., 2013).
471 These findings are in line with papers reporting a negligible sensitivity to pH for perfect, defect free
472 graphene sheets (Fu et al., 2011). Nevertheless, a consistent explanation of the pH response of
473 carbon nanomaterials is still lacking.

474 Recently, ink-jet printing was used to deposit –COOH functionalized SWCNTs on glass and polymeric
475 substrates, obtaining a potentiometric sensor. A linear response, with slope related to the number of
476 layers, was recorded in the pH range 3 – 11 (Qin et al., 2016). Carbon nanotubes can also be
477 integrated into traditional semiconductor-based electronics for the realization of transistor-like devices
478 with sensing properties. An extended gate FET (EGFET) was realized with a CNT network (Chien et
479 al., 2012) employed for both the contact electrode and the sensing membrane. The CNTs were first
480 acid-oxidized and then irradiated with a laser beam to increase the defect concentration on their
481 surface. This treatment resulted in a greater sensitivity (50.9 mV/pH) of the FET to pH and in a good
482 linearity (Correlation coefficient R^2 : 0.998) of the response.

483 Similarly, most graphene based sensors are, realized as transistors. Ohno et al. (2009) reported on
484 the fabrication of a solution-gated FET (SGFET) made by a single layer of mechanically exfoliated
485 graphene onto SiO₂/silicon substrate. The charge transport properties of the graphene layer depend
486 on pH and a nearly linear correlation was found between the gate potential (measured at the Dirac
487 point) and pH, with a sensitivity of approximately 30 mV/pH. For the same kind of device (Ohno et al.,
488 2010), the authors analyzed the signal/noise parameters in a narrower pH range (5 – 8) and
489 calculated a promising detection limit of 0.025. Using a different approach, few-layer graphene
490 (thickness 1-2 or 3-4 layers) was grown epitaxially on silicon to realize a SGFET, tested in the pH
491 range 2 – 12. Interestingly, a super-Nernstian sensitivity of 99 mV/pH was recorded, irrespective of
492 the thickness (Ang et al., 2008). The authors performed impedance spectroscopy to rule out any
493 external influence on the conduction behaviour of the device, demonstrating that only the adsorption
494 of OH⁻ / H₃O⁺ species determines the properties.

495 One of the interesting advantages of carbon nanomaterials is the possibility to use conventional
496 fabrication techniques to realize electronic devices and sensors on flexible substrates (Jung et al.,
497 2014; Sharma & Ahn, 2013). Single wall nanotubes were employed for the fabrication of flexible FETs
498 supported on polyethylene terephthalate (PET) films, using a layer-by-layer (LbL) approach. The film
499 was obtained by LbL deposition of carboxylated SWCNT with two polyelectrolites, to work as the gate
500 electrode. The response of the FET was found to be dependent on pH, although in a non-linear way
501 (Lee & Cui, 2010). Mailly-Giacchetti et al. (2013) transferred graphene layers, grown by CVD, onto
502 poly(ethylene 2,6-naphthalenedicarboxylate) (PEN), silicon modified with octadecyltrichlorosilane
503 (OTS) and SiO₂, to evaluate the influence of the substrate on sensing. Although the different devices
504 showed different conductivities, the sensitivity to pH was around 22 mV/pH for all of them.

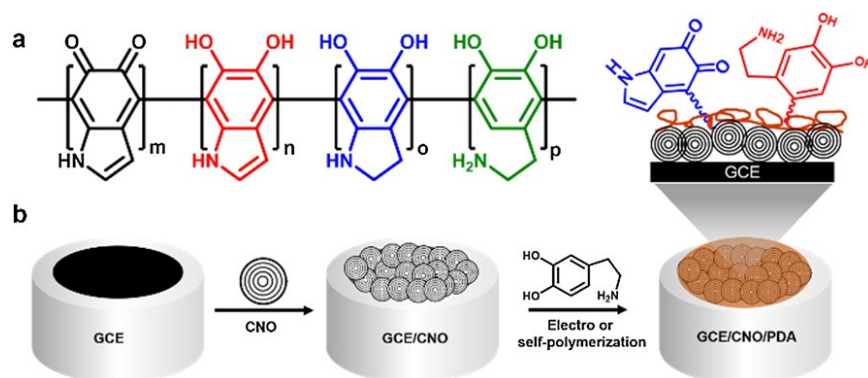
505 Some refinements in the design of graphene devices have been proposed to improve the sensing
506 performance. A suspended graphene FET was fabricated with a claimed increase in the signal to
507 noise ratio by 14 dB with respect to the same unsuspended device (Cheng et al., 2010). The increase
508 in signal quality allowed measurements to be carried out with very low applied voltage, reducing the
509 risk of interference from the testing solution (polarization, redox reactions). An interesting approach to
510 increase the contact surface with the aqueous solution has been recently proposed by Ameri et al.
511 (2016) with the realization of a high porosity graphene foam covered by a thin layer of HfO₂. This
512 device was tested in Dulbecco phosphate buffer, showing a super Nernstian sensitivity of 71 mV/pH
513 and a fast response. Finally, a solid gated G-FET designed to avoid the need for an external
514 reference electrode was reported. In this device, a layer of HfO₂ is deposited between the graphene
515 layer and a gold gate electrode (Zhu et al., 2015). The response of the FET was linear with pH in the
516 range 5.3 – 9.1, with a sensitivity of 56.5 mV/pH.

517 GO and rGO materials can be used for the fabrication of membranes and networks, showing lower
518 electrical properties compared to graphene but better pH sensitivity, probably due to the high
519 concentration of oxidized groups (Sohn et al., 2013). A potentiometric GO based sensor has been
520 realized for medical applications by printing the electrodes on a plastic substrate (Salvo et al., 2017)
521 and calibrated in a buffer with isotonic salt concentration. The potential response to pH was linear and
522 the sensors proved to be relatively stable for 1 week in serum. A sensor for seawater pH detection
523 was derived from this system (Poma et al., 2019) and validated in high ionic strength buffers and real
524 seawater. GO and rGO electrodes were coated with Nafion to increase stability and tested, with rGO
525 (functionalized with 4-aminofenilacetic acid) showing the highest sensitivity. Stability was assessed for
526 up to 8 days in seawater but the accuracy of the sensor was worse than the reference glass
527 electrode.

528 Nanomaterials are often combined with polymeric substrates/matrices, for processing reasons and to
529 enhance sensing performance by exploiting the synergism between the components. Synergistic
530 effects can be observed in carbon nanomaterials combined with conducting polymers: the polymer
531 increases the robustness and selectivity of the response; at the same time, the incorporation of
532 nanoparticles improve the stability and the conductivity of polymers, enhancing the electric properties.
533 Polyaniline is by far the most studied conducting polymer for the development of composites (Oueiny
534 et al., 2014). Interesting results have been obtained by Loh et al. (2007), by combining CNTs with a
535 conducting layer-by-layer thin film of PSS/PANI and employing the assembly in a resistive pH sensor.
536 The electrical resistance showed a large shift upon pH change (pH 1 to 10), with a sensitivity of
537 approximately 19.9 kΩ cm⁻²/pH. Similarly, Boeva et al. (2014) produced few-layer graphene and
538 exfoliated (30 – 50 layers) graphite coated by PANI. The redox behaviour of these materials was
539 investigated by cyclic voltammetry, showing that PANI nanocomposite preserve their electroactivity up
540 to neutral pH due to interactions with the graphene, whereas neat PANI loses its conductivity above
541 pH 3. A miniaturized pH meter based on amino-functionalized graphene/PANI nanocomposite was
542 fabricated by electropolymerization on ITO/glass substrate and tested by voltammetric measurements
543 in PBS buffer, resulting remarkably stable up to pH 11 (Su et al., 2016). Similarly, very stable sensing
544 performance was also recorded on polyaniline functionalized rGO, tested in both potentiometric and

545 resistive setup in the range 2 – 9. The PANI-rGO electrodes were coated with a Nafion film to
 546 decrease interference from other ions and tested in a L. Lactis fermentation reactor (Chinnathambi &
 547 Euverink, 2018). Recently, Grozdanov et al. (2018, 2019) have tested screen printed electrodes
 548 (SPE) modified with PANI/carbon nanotubes composites as pH nanosensors, in the frame of FP7
 549 project COMMON SENSE (Cleary et al., 2014; Barton et al., 2016; Ribotti et al., 2015). Nanosensors
 550 were prepared by electropolymerization and exhibited a high value of conductivity, which was
 551 attributed to the synergistic effect of the conductive polymer and carbon nanostructure via π - π
 552 stacking. Conductivity changes were measured at different pH (4 to 10) in commercial buffers, as well
 553 as in seawater samples showing a non linear response to pH. Similar electrodes were produced by
 554 Bao et al. (2019), who produced a PANI/MWCNT ink for screen printing of miniaturized working
 555 electrodes. Here, the response was measured by chronoamperometry, observing a linear relationship
 556 of potential vs. pH in the range 2 – 11; the role of nanotube/PANI interactions in the enhancement of
 557 the electric response was pointed out. Amperometric pH sensors were produced (Sha et al., 2017) by
 558 electropolymerization of well-ordered PANI chains on graphene-modified carbon electrodes, showing
 559 a nearly linear response to pH. The sensitivity was higher in alkaline solutions, which is rarely
 560 observed for PANI due to the dependence of electroactivity on acid doping.

561 A number of other polymers have been used for nanocomposite sensors fabrication. Gou et al.
 562 (2014). deposited a layer of oxidized SWCNTs between gold electrodes onto a silicon substrate, then
 563 poly(1-amino anthracene, PAA) was electropolymerized onto CNTs. The obtained device was tested
 564 in either liquid gated FET or conductometric configuration in various pH, showing high sensitivity and
 565 stability of the response over long time. The detection limit (resolution) is 0.04 pH. Recently, a
 566 biomimetic polymer, polydopamine (PDA), has also shown redox properties (Amiri et al., 2016) and,
 567 thanks to its excellent adhesion properties, has been used to modify nanostructured carbon
 568 electrodes (Figure 5; Zuaznabar-Gardona & Frago, 2018). PDA response was investigated by both
 569 cyclic voltammetry and potentiometry, showing a higher sensitivity when combined with carbon
 570 nanostructures, up to 53 mV/pH. The electrodes were stable for several months in water and only
 571 attacked by strong alkaline solutions. They were also tested in seawater showing a very good
 572 agreement with the reference pH meter.



573

574 **Figure 5.** General structure of polydopamine (a) and schematic fabrication of nano-onions (CNO) and
 575 polydopamine (PDA) deposition on glassy carbon electrodes (GCE) (b). Reprinted from Zuaznabar-Gardona and
 576 Frago (2018), with permission from Elsevier.

577 As a further example of polymer/nanoparticle synergism, it is worth mentioning the design proposed
 578 by Crespo et al. (2009). An acrylic ion selective membrane, doped to increase the selectivity towards
 579 H⁺ ions, was cast on a MWCNT-modified carbon electrode and tested for potentiometric pH
 580 measurements. Nanotubes here are introduced as a solid contact between the polymeric membrane,
 581 exhibiting pH dependent ionic conduction, and the working electrode. The result is a sensor with
 582 Nernstian response and high selectivity. The design of this kind of sensor has been refined over the
 583 years leading to the fabrication of a complete apparatus for field testing campaigns in freshwater
 584 (Athavale et al., 2017) and, notably, in seawater (Cuartero et al., 2017) showing sensing performance
 585 comparable with commercial sensors.

586 **Table 4.** pH sensors based on nanostructured polymers, carbon nanomaterials and their combination. In bold,
 587 sensors that have been tested in seawater.

Sensing material and setup	Testing range and media	Sensitivity	Stability	Response time	Reference
Polypyrrole NW ISFET	1 – 11 Commercial buffers	0.4/pH (normalized drain current)	n/a	Few s	Shirale et al., 2010
Polypyrrole NW array Potentiometric	2 – 12	Up to 49.3 mV/pH	Stable up to 50 d of storage	n/a	Sulka et al., 2013
PANI nanofibers Potentiometric	3 – 10 Commercial buffers High selectivity against common cations	62.4 mV/pH	Drift of 3 mV/h over 15 h	12.8 s	Park et al., 2019
PANI nanopillars Potentiometric	2 – 12 Commercial buffers Negligible effects of Na ⁺ , K ⁺ , NH ₄ ⁺ , Ca ²⁺ , and Mg ²⁺ at 10 mM	60.3 mV/pH	Low drift (0.64 mV/h) during a 15 h test	5 s	Yoon et al., 2017
PANI particles in epoxy Resistive	2.4 – 10 Commercial buffers	957 μS/pH	Stable within 4% for 30 d (tested every 5 d)	5 – 30 s	Patil et al., 2019
SWCNT-COOH Potentiometric	3 – 11 Britton-Robinson buffer	48.1 ± 0.4 mV/pH	Response is reduced by 4% after 15 d of storage	7 s	Qin et al., 2016
MWCNT-COOH EGFET	3 – 13 PBS	50.9 mV/pH	n/a	n/a	Chien et al., 2012
Single graphene layer on SiO ₂ Solution gated FET	4 – 8.2 10 mM phthalate, phosphate and borate buffers	Approx. 30 mV/pH Resolution is 0.025 pH units	n/a	n/a	Ohno et al., 2009, 2010
Single graphene layer on PEN Solution gated FET	4 – 9 Phosphate buffer adjusted with strong acids/alkali	22 mV/pH	Response decrease after exposure to acid solutions	≈ 10 min	Maily-Giacchetti et al., 2013
Graphene foam coated with HfO ₂ Solution gated FET	3 – 9 Dulbecco buffer adjusted with strong acids/alkali	71 ± 7 mV/pH	n/a	≤ 240 s	Ameri et al., 2016
Graphene + HfO ₂ dielectric layer	5.3 – 9.2	56.5 mV/pH	n/a	< 60 s	Zhu et al., 2015

FET	Phosphate saline buffer				
rGO Solution gated FET	6 – 9 Phosphate buffer	29.2 mV/pH	n/a	Few s	Sohn et al., 2013
GO Potentiometric	4 – 10 Citrate, borate, phosphate buffers (isotonic) Tested in human serum	40 ± 4 mV/pH	Negligible drift over 1 h in buffers. Stable for 1 w in serum	n/a	Salvo et al., 2017
Reduced GO + Nafion membrane Potentiometric	4 – 10 Citrate, borate, phosphate Tested in superficial seawater	45 mV/pH	Fluctuations observed in the response over 56 h in buffers. Signal stable for 8 d in seawater	n/a	Poma et al., 2019
Graphene platelets Resistive	1 – 10 Commercial buffers	19.9 (k Ω /cm ²)/pH Poor linearity	n/a	n/a	Loh et al., 2007
Amino functionalized graphene / PANI Voltammetry	1 – 11 PBS	51.1 mV/pH	Response decrease after 1 w	n/a	Su et al., 2016
rGO/PANI + Nafion membrane Potentiometric Resistive	2 – 9 Britton-Robinson buffer Also tested in a bacterial fermentation broth	55 mV/pH 1.71 Ω /pH	n/a	n/a	Chinnathambi & Euverink, 2018
PANI-MWCNT Chronoamperometry	2 – 11 Water adjusted with HCl/NaOH	20.6 mV/pH	n/a	Few s	Bao et al., 2019
PANI on graphene-carbon electrode Amperometric	1 – 11 NaCl solution adjusted with HCl, H ₃ PO ₄ , NaOH	50.17 μ A/(pH cm ²) for pH 1 – 5 139.2 μ A/(pH cm ²) for pH 7 – 11	n/a	≈ 100 s	Sha et al., 2017
SWCNT – PAA Solution gated FET / Conductometric	2 – 12 Britton-Robinson buffers Response to Na ⁺ and Ca ⁺ negligible	0.073 mS/pH	Stable for ≈ 2 h (no drift). Same sensitivity after 120 d of storage	≈ 60 s	Gou et al., 2014
Polydopamine/carbon nano-onions Potentiometric	1.5 – 10.5 Universal buffer Tested in seawater (pH 8.3) Low interference of alkaline cations	53 mV/pH	Stable over 4 w	15 s	Zuaznabar-Gardona & Fragoso, 2018
MWCNT solid contact + acrylic membrane Potentiometric	3 – 10 Various buffers Lake freshwater Tested in seawater (pH 7.9 – 8) Selective against alkali cations and sulfides	58.8 ± 0.4 mV/pH	Estimated drift 0.1 mV/h	10 s	Athavale et al., 2017; Cuartero et al., 2017

589 Three of the pH sensors listed in Table 4 have been recently tested in seawater, while most of the
590 published works on sensors based on carbon-based nanomaterials only tested the sensors in
591 buffered solutions. The first consists of a graphene-based pH sensor, part of an autonomous system
592 for the remote monitoring of pH and temperature at sea (Poma et al., 2019); the pH measurement is
593 performed through a potentiometric sensor with a wireless, smartphone-based real time acquisition
594 system. The pH sensor was validated in the laboratory, using seawater samples, then it was deployed
595 at sea for 8 days recording one pH reading per hour. In both cases, a commercial glass electrode pH-
596 meter was used as a reference device. Results between this versatile, low-cost system and the
597 reference commercial glass pH electrode were comparable for both laboratory and in-field
598 experiments. In addition, this graphene-based system also exhibited lower energy consumption and
599 greater calibration stability than the commercial glass electrode. The second pH sensor is again
600 potentiometric like the first one but based on polydopamine (PDA) films coated on a carbon nano-
601 onion conductive surface. Also in this case, the new pH sensor was validated through comparison
602 with a commercial glass pH electrode coupled to a pH meter from the same builder in water sampled
603 at sea. They showed an excellent correspondence between these new PDA pH sensors and
604 commercial ones with the advantages of an easy fabrication, an excellent reproducibility, a stability of
605 the PDA coating in water over several months and the possibility of its integration into miniaturized
606 devices. Both the potentiometric pH sensors described above must be tested in the field for longer
607 times in order to verify stability and the long term effects e.g. of biofouling on system performance.
608 The last example of a potentiometric sensor successfully tested in freshwater (Athavale et al., 2017)
609 and in seawater (Cuartero et al., 2017), is based on an acrylic ion selective membrane with a carbon
610 nanotube solid contact layer. For tests in seawater, the sensor was deployed in different coastal
611 marine environments: Arcachon Bay on the Atlantic French coast for 14 hours, Genoa harbor on the
612 Italian Mediterranean coast for 58 and 167 hours, and a mix sea-freshwater effluent, the Eyre River,
613 in the Arcachon Bay during high tides for 14 hours. In all these tests the sensor showed good
614 agreement with a reference glass electrode. This was particularly evident during the tests inside the
615 harbour of Genoa where the sensor was compared with that mounted on a commercial
616 multiparametric or Conductivity Temperature Depth (CTD) probe.

617 **5.2 Semiconductor and metal/metal oxide nanomaterials**

618 The most traditional of semiconductor materials, silicon, has found new interesting applications in
619 sensing with the development of Si nanowires (NW). Nanostructures with high packing density and
620 tailored spacing can be fabricated by electron beam lithography on a silicon-on-insulator substrate
621 with high accuracy and reproducibility (Bedner et al., 2013; Park et al., 2010). Choi et al. (2012)
622 produced NWs on boron-doped silicon and deposited a protective layer of Si_3N_4 to ensure better
623 stability. The resistivity of the NW was measured as a function of pH and both short-time noise and
624 long-term drift were measured (Choi et al., 2012). The pH sensitivity of this NW based device has
625 been attributed to charge accumulation at the surface that induces a change in carrier density into the
626 high surface area wires, affecting conductivity. Recently Kim et al. (2014) produced As-doped
627 suspended NWs by a lithographic approach. A linear correlation between normalized conductance
628 and pH was found in the range 4 – 8, with a slope of 0.3 that is twice the slope of non-suspended

629 nanowires (Table 5). The sensitivity was found to exceed the theoretical Nernst limit and, depending
630 on the working current chosen, varied between 87 and 103 mV/pH (Salaün et al., 2014). This
631 unexpected behaviour was observed also in double-gate NW transistors (Ahn et al., 2013) and
632 rationalized taking into account the capacitance of the gates themselves (Knopfmacher et al., 2010).
633 Finally, it is worth reporting a different application of Si NW, grown as a dense array to modify the
634 gate of a FET device. The wires were sputtered with indium-gallium-zinc oxide (IGZO) resulting in a
635 sensitivity of 50 mV/pH (Lin et al., 2013) at a working current of 200 μ A.

636 Metal oxide nanostructures can be produced by means of various fabrication techniques, exhibiting
637 interesting electrochemical properties. An example is nanometric sulfated iron oxide (Alizadeh &
638 Jamshidi, 2015). The particles produced by sol-gel were supported with a carbon paste and heat
639 treated at 600°C to produce a regular crystal structure. With an optimized structure, the sensitivity
640 was 57.5 mV/pH and a stability of 1 week was observed, providing the electrode is stored in water or
641 immersed for a few hours in water after storage in dry conditions. Many other semiconducting metal
642 oxides with very interesting properties can be shaped into nanometric wires, ribbons or tubes by
643 different techniques and, interestingly, they can be easily integrated with well established silicon
644 technologies. Titanium and zinc oxide nanotubes/wires are probably the most tested nanomaterials
645 for pH sensing. Both materials show an amphoteric behaviour and can be used in both acidic and
646 alkaline media; the active sites for sensing are oxygen vacancies found at the surface of the oxide
647 structures. Titania nanotubes (NT) with lengths ranging from 33 to 800 nm were produced by
648 anodization of a titanium electrode and embedded in PDMS for testing (Zhao et al., 2010). A nearly
649 Nernstian behaviour was recorded for the nanotube modified electrodes, with best sensitivity and
650 linearity obtained with amorphous titania. Materials prepared in different anodization conditions to
651 produce a dense and thick nanotube layer onto titanium electrodes showed that the production
652 parameters can affect the potentiometric response vs. pH (Albertin et al., 2013). To increase chemical
653 stability, titania can be converted to nitride (TiN), producing a dense array of NTs onto platinum
654 electrodes (Liu et al., 2016). TiN showed a higher pH sensitivity with respect to TiO₂, excellent
655 reproducibility and a good stability over 1 month of storage.

656 Fulati et al. (2009) produced zinc oxide nanotubes and wires, growing them onto gold substrates from
657 a zinc nitrate solution. The response at different pH was measured showing a higher sensitivity for the
658 NTs, explained in terms of higher surface area, and stability of the signal over several days. ZnO
659 nanostructures are increasingly investigated for miniaturized devices (Kumar et al., 2019) and in
660 particular for medical applications (Young & Tang, 2019). A linear response was recorded in the pH
661 range 2 – 12 with aluminium-doped zinc oxide nanosheets (Tsai et al., 2019), tested as the gate layer
662 of an ISFET.

663 A large number of nanostructured oxides have been exploited for pH sensing in different
664 configurations, with a recent trend towards the realization of low cost, flexible devices. High
665 crystallinity tin oxide (SnO₂) nanorods have been produced by a low temperature process onto
666 conductive ITO glass (Li et al., 2012), and this layer was employed as a sensitive gate in an EGFET
667 device. The sensitivity was increased with respect to thin film devices in both the linear and saturation

668 regions of the transistor. Moreover, this device showed low hysteresis and no signal degradation
669 during many hours of operation. Ruthenium oxide nanoparticles, deposited on a plastic supported
670 electrode, have been tested as pH sensitive material in an EGFET configuration (Singh et al., 2019).
671 The device showed a super-Nernstian behaviour, not usually observed for this oxide and a
672 stabilization of the observed drift after 8 hours. Nanostructured platinum electrodes were realized by
673 ink-jet printing onto a plastic substrate by Zea et al. (2019) and modified by electrodeposition of a thin
674 IrO_x amorphous layer. The flexible devices were tested in the pH range 2 – 11 and aged in both dry
675 and wet conditions over 1 year, showing excellent stability.

676 Tungsten oxide (WO₃) is gaining increasing attention as a pH sensitive material. A WO₃ layer was
677 deposited by Zhang and Xu (2009) on a nanostructured electrode composed by aligned CNTs,
678 obtaining a sort of nanopillar. Such modified electrodes showed a sensitivity of about 41 mV/pH, a low
679 drift rate and a good stability after 1 month of storage. Tungsten oxide nanoparticles deposited onto a
680 flexible, plastic supported electrode, showed a linear potential response to pH in the range 5 – 9
681 (Santos et al., 2014). A reduction of the sensitivity was however observed with continuous operation
682 at different pH over ≈ 1 h. The same material was deposited onto glassy carbon to realize a sensor for
683 voltammetric measurement of pH (Jamal et al., 2019), obtaining a high sensitivity (60 mV/pH) and
684 linearity of the response. Drift was observed during the initial hours of sensor testing, but the signal
685 stabilized thereafter remaining stable for up to 7 days. Recently, Choi et al. (2019), reported a new
686 type of potentiometric pH sensor based on 1D tungsten oxide nanofibers with an amplified signal
687 exceeding the Nernstian limit. Nanofibers with high porosity were synthesized and stabilized in a
688 chloromethylated triptycene poly (ether sulfone) matrix, allowing a fast proton diffusion into the
689 composite membrane. A high pH sensitivity of -377.5 mV/pH was obtained with the amplified sensor,
690 linearity was acceptable in a narrow pH range (6.9 – 8.9). Testing in artificial seawater demonstrated
691 a negligible effect of dissolved ions.

692 The advantages of nano-scale dimensions can also be exploited, in combination with organic support
693 and/or ion-selective layers, for the realization of multicomponent sensing systems. An ISFET was
694 realized by LbL deposition, using poly(diallyl dimethylammonium) (PDDA) and poly(styrene sulfonate)
695 (PSS) embedding alternate layers of silica and In₂O₃ nanoparticles (Liu & Cui, 2007). The
696 semiconducting indium oxide granted a sufficient conductivity to the device while the protonation/
697 deprotonation of SiO₂ is responsible for pH sensing. A parabolic dependence of current vs. pH was
698 recorded, with higher sensitivity in acid solutions. A development of this concept led to the realization
699 of reliable and sensitive pH sensors based on the LbL assembly of iridium oxide nanoparticles and
700 PDDA. The sensors produced showed a fast response and excellent reproducibility, by using a very
701 low amount of iridium, paving the way for low cost, robust disposable sensors (Jović et al., 2018).
702 Another example of synergistic combination of conducting polymer and nanoparticles was proposed
703 by Kim et al. (2016), who developed a poly(terthiophene benzoic acid) (pTBA) / nanostructured
704 AuZnO_x composite for disposable, solid state pH sensors. These devices were calibrated in the range
705 2 – 12 and showed fast response and stability when tested in biological samples. Lenar et al. (2019)
706 recently proposed RuO₂ nanoparticles showing low resistivity, high stability and redox behaviour, as a
707 solid contact layer between a carbon electrode and a modified PVC-based H⁺ selective membrane.

708 The assembly showed a fast, Nernstian response, largely due to the performance of oxide
 709 nanoparticles in synergy with the selectivity provided by the polymeric membrane.

710 **Table 5.** pH sensors based on semiconductor and metal/metal oxide nanomaterials. In bold, sensors that have
 711 been tested in seawater.

Sensing material and setup	Testing range and media	Sensitivity	Stability	Response time	Ref.
Si nanowire + Si ₃ N ₄ passivation layer ISFET	4 – 9 HCl and KOH solutions	5.4%/pH	Maximum drift of 1.68% at pH = 9	n/a	Choi et al., 2012
Si suspended nanowire ISFET	4 – 8 PBS buffer adjusted with HCl and NaOH	0.3/pH (expressed as relative conductance $\Delta G/G_0$)	n/a	n/a	Kim et al., 2014
Polycrystalline Si nanowire ISFET	4 – 9.2	Up to 103 mV/pH	n/a	n/a	Salaün et al., 2014
Si NW Double gated FET	4 – 10 PBS buffer	69 mV/pH	Drift of 27 mV/h	n/a	Ahn et al., 2013
Si NW sputtered with IGZO ISFET	2 – 10	50 mV/pH	n/a	Few seconds	Lin et al., 2013
Fe ₂ O ₃ nanoparticles Potentiometric	1.5 – 12.5 Negligible influence of common cations	57.5 mV/pH Hysteresis effects \leq 6%	Stable for > 1 w of storage. Surface can be renewed by rubbing with paper. Reconditioning at pH=7 for few h is needed	\approx 10 s	Alizadeh & Jamshidi, 2015
TiO ₂ nanotubes Potentiometric	2 – 12 Britton-Robinson buffer Negligible interference of common ions (Na ⁺ , K ⁺ , Cl ⁻ , NO ₃ ⁻ , SO ₄ ²⁻ , F ⁻ , I ⁻ , Fe(CN) ₆ ⁴⁻)	Up to 59 mV/pH (54 mV/pH before UV irradiation)	n/a		Zhao et al., 2010
TiN nanotubes Potentiometric	2 – 11 Britton-Robinson buffer Low effect of monovalent cations and F ⁻	55.3 mV/pH	Negligible drift over 200 s. Stable after 1 month storage	4.4 s	Liu et al., 2016
ZnO nanotubes Potentiometric	4 – 12 Commercial buffers Response influenced by CaCl ₂	45.9 mV/pH	Up to 5 d (tested at day 0, 2 ad 5)		Fulati et al., 2009
Al-doped ZnO ISFET	2 – 12 Commercial buffers	\approx 50 mV/pH	Stable for 12 w at pH 2	0.3 s	Tsai et al., 2019
SnO ₂ nanorods EGFET	1 – 13 Commercial buffers	55.2 mV/pH (linear regime) 0.86 μ A/pH (saturation regime)	Up to 6 h continuous operation	n/a	Li et al., 2012
RuO ₂ nanomembrane EGFET	2 – 12 Commercial buffers	65.1 mV/pH (linear regime) 1.05 μ A/pH	Drift of 2 mV/h, stabilizes after 8 h of immersion	n/a	Singh et al., 2019

	Low interference of mono and divalent cations	(saturation regime)			
IrO _x onto nanostructured Pt Potentiometric	2 – 11 KCl solution adjusted with strong acid/base	70.9 mV/pH Standard deviation < 1%.	Stable for 1 year, dry or immersed in PBS. Sensitivity stabilizes after 1 month	6 – 8 s	Zea et al., 2019
WO ₃ layer on CNTs Potentiometric	2 – 12 Britton-Robinson buffer	40.73 mV/pH	Standard error < 1% Stable after 1 month of storage	30 s (pH 4) 90 s (pH 12)	Zhang & Xu, 2009
WO ₃ nanoparticles Potentiometric	5 – 9 Commercial buffers	56.7 ± 1.3 mV/pH	Sensitivity reduction over time	28 s	Santos et al., 2014
WO ₃ nanoparticles Voltammetry	3 – 11 Phosphate buffer Tested in vinegar	60.0 ± 0.01 mV/pH	Average drift of 33 mV over 3 h. 95% sensitivity retained after 7 d of use	n/a	Jamal et al., 2019
WO ₃ nanofibers Potentiometric, amplified	3 – 11 Commercial buffers Tested in artificial seawater (pH 8.0 – 7.6)	38.9 mV/pH (amplified to 377.5 mV/pH)	n/a	n/a	Choi et al., 2019
IrO _x / PDDA Potentiometric	3 – 10 Commercial buffers	59 mV/pH	n/a	3 s	Jović et al., 2018
pTBA / AuZnOx Potentiometric	2 – 13 Commercial buffers Also tested in saliva and urine samples	59.2 ± 0.5 mV/pH	Stable for cyclic measurements (200 s). Good stability upon storage for 15 d	1 s	Kim et al., 2016
RuO ₂ np solid contact + PVC based membrane Potentiometric	2 – 12 Tris buffer High selectivity against monovalent cations	59 mV/pH	Stable for 1 w of daily calibrations	n/a	Lenar et al., 2019

712

713 None of the potentiometric pH sensors listed in Table 5 was tested in seawater apart from the WO₃
714 nanofibers potentiometric amplified sensor realized by Choi et al. (2019). They tested such sensors in
715 artificial seawater and calibrated the reading against a commercial pH meter. Due to the high
716 sensitivity obtained through the amplification, the authors concluded that their new pH sensor is
717 promising for portable and low-cost applications for the monitoring of seawater; however, stability and
718 long term performance were not assessed.

719

720 6. Conclusions

721 pH is a key parameter in many chemical, biological and biogeochemical phenomena and is of
722 particular interest in environmental monitoring. Ion sensitive glass electrodes are the most used
723 sensors for pH measurements, but new solutions for the realization of robust, precise and affordable
724 pH sensors are actively investigated.

725 In this review, we have presented the most recent developments in pH sensing materials, reporting
726 sensor performance and main parameters. Solid state sensors based on inorganic materials, (metals
727 of semiconductors), and carbon based materials (polymers and carbon particles) have been
728 reviewed, revealing a general trend towards the realization of miniaturized, low cost/disposable
729 sensors.

730 The development of nano-engineered materials and composites as active sensing elements has
731 emerged as a promising strategy to improve sensitivity, response time, flexibility and ease of
732 fabrication. Thin films and nanomaterials based on metal oxides provide good sensing performance
733 and relatively good stability and can be easily integrated in potentiometric sensors or silicon-based
734 FET devices. Examples of application of metal oxide pH sensors in different environments, including
735 seawater, have been reported pointing out their robustness and flexibility.

736 Carbon nanoparticles, despite having attracted a large research effort, are not stable in their response
737 (sensitive to surface defects, functional groups and morphology), nor easy to produce and handle.
738 Polymer-based sensors, finally, seem to be non-competitive in terms of precision and stability.
739 However, the limitations shown by these classes of materials can be overcome by properly combining
740 them. In this respect, the synergy observed between polymeric components, and inorganic
741 nanomaterials seems to be a key factor for the realization of robust and affordable sensors. Polymers
742 can be used as efficient ion-selective or protective elements, to enhance the response of inorganic
743 sensing elements and decrease the interference of dissolved ions. On the other hand, the response
744 and the stability of pH sensitive polymers can be greatly improved by combining them with conductive
745 and semiconductive nanomaterials, as shown for the most common electroactive polymer, PANI, and
746 for polydopamine.

747 For each sensor class, results of testing in seawater, when available, have been reported and
748 discussed. Only few new sensors have been designed for seawater, however, the examples reported
749 show promising results in terms of sensitivity, selectivity vs. interfering ions and stability. While some
750 inorganic materials (metal oxides) have shown good sensing performance at sea, among the devices
751 based on polymers or carbon nanomaterials the only ones successfully tested in seawater are based
752 on composite or multilayer structures. Design refinement and extensive field testing and validation are
753 needed to assess the suitability of the sensors presented for seawater monitoring. Even if the
754 possibility to replace well-established measurement technologies like glass electrodes and
755 spectrophotometry is currently unrealistic, in the near future, robust, miniaturized, integrated arrays of
756 solid state electrochemical pH sensors can represent a valuable alternative for specific applications.

757

758 **Acknowledgments.** We gratefully acknowledge funding received from the European Union's Seventh
759 Framework Programme (FP7) for research, technological development and demonstration (OCEAN
760 2013.2) under grant agreement No. 614155. We also thank the three anonymous reviewers whose
761 comments/suggestions helped improve and clarify this manuscript.

762 **References**

- 763 Adhikari, B., & Majumdar, S. (2004). Polymers in sensor applications. *Progress in Polymer Science*,
764 29(7), 699–766. doi: 10.1016/j.progpolymsci.2004.03.002
- 765 Ahn, J.-H., Kim, J.-Y., Seol, M.-L., Baek, D.J., Guo, Z., Kim, C.-H., Choi, S.-J., & Choi, Y.-K. (2013). A
766 pH sensor with a double-gate silicon nanowire field-effect transistor. *Applied Physics Letters*, 102,
767 083701. doi: 10.1063/1.4793655
- 768 Albertin, K.F., Carreño, M.N.P., & Pereyra, I. (2013). Study of TiO₂ Nanotubes for Sensors and
769 Integrated Devices. *Precision Instrument and Mechanology*, 2(3), 114-121.
- 770 Alizadeh, T., & Jamshidi, F. (2015). Synthesis of nanosized sulfate-modified α -Fe₂O₃ and its use for
771 the fabrication of all-solid-state carbon paste pH sensor. *Journal of Solid State Electrochemistry*,
772 19, 1053–1062. doi: 10.1007/s10008-014-2716-4
- 773 Ameri, S.K., Singh, P.K., & Sonkusale, S.R. (2016). Three dimensional graphene transistor for ultra-
774 sensitive pH sensing directly in biological media. *Analytica Chimica Acta*, 934, 212-217. doi:
775 10.1016/j.aca.2016.05.048
- 776 Amiri, M., Amali, E., Nematollahzadeh, A., & Salehniya, H. (2016). Poly-dopamine films: Voltammetric
777 sensor for pH monitoring. *Sensors and Actuators B: Chemical*, 228, 53–58. doi:
778 10.1016/j.snb.2016.01.012
- 779 Ang, P.K., Chen, W., Wee, A.T.S. & Ping, K. (2008). Solution-Gated Epitaxial Graphene as pH
780 Sensor. *Journal of the American Chemical Society*, 130, 14392–14393. doi: 10.1021/ja805090z
- 781 Ates, M. (2013). A review study of (bio)sensor systems based on conducting polymers. *Materials*
782 *Science and Engineering C*, 33(4), 1853–1859. doi: 10.1016/j.msec.2013.01.035
- 783 Athavale, R., Dinkel, C., Wehrli, B., Bakker, E., Crespo, G.A., & Brand, A. (2017). Robust solid-
784 contact ion selective electrodes for high-resolution in situ measurements in fresh water systems.
785 *Environmental Science and Technology Letters*, 4(7), 286-291. doi: 10.1021/acs.estlett.7b00130
- 786 Back, J.H., & Shim, M. (2006). pH-Dependent Electron-Transport Properties of Carbon Nanotubes.
787 *Journal of Physical Chemistry B*, 110, 23736-23741. doi: 10.1021/jp063260x
- 788 Bangar, M., Chen, W., Myung, N., & Mulchandani, A. (2010). Conducting polymer 1-dimensional
789 nanostructures for FET sensors. *Thin Solid Films*, 519, 964-973. doi: 10.1016/j.tsf.2010.08.023
- 790 Banna, M.H., Najjaran, H., Sadiq, R., Imran, S.A., Rodriguez, M.J., & Hoorfar, M. (2014). Miniaturized
791 water quality monitoring pH and conductivity sensors. *Sensors and Actuators B: Chemical*, 193,
792 434-441. doi: 10.1016/j.snb.2013.12.002
- 793 Bao, Q., Yang, Z., Song, Y., Fan, M., Pan, P., Liu, J., Liao, Z., & Wei, J. (2019). Printed flexible
794 bifunctional electrochemical urea-pH sensor based on multiwalled carbon nanotube/polyaniline
795 electronic ink. *Journal of Materials Science: Materials in Electronics*, 30(2), 1751-1759. doi:
796 10.1007/s10854-018-0447-5

797 Barton, J., Begoña González García, M., Hernández Santos, D., Fanjul-Bolado, P., Ribotti, A.,
798 McCaul, M., Diamond, D., & Magni P. (2016). Screen-printed electrodes for environmental
799 monitoring of heavy metal ions: a review. *Microchimica Acta*, 183, 503-517. doi: 10.1007/s00604-
800 015-1651-0

801 Bedner, K., Guzenko, V.A., Tarasov, A., Wipf, M., Stoop, R.L., Just, D., Rigante, S., Fu, W.,
802 Minamisawa, R.A., David, C., & Calame, M. (2013). pH response of silicon nanowire sensors:
803 impact of nanowire width and gate oxide. *Sensors and Materials*, 25(8), 567-576. doi:
804 10.18494/SAM.2013.890

805 Bergveld, P. (2003). Thirty years of ISFETOLOGY: What happened in the past 30 years and what
806 may happen in the next 30 years. *Sensors and Actuators B: Chemical*, 88(1), 1–20. doi:
807 10.1016/S0925-4005(02)00301-5

808 Boeva, Z.A., Milakin, K.A., Pesonen, M., Ozerin, A.N., Sergeyev, V.G., & Lindfors, t. (2014).
809 Dispersible composites of exfoliated graphite and polyaniline with improved electrochemical
810 behaviour for solid-state chemical sensor applications. *RSC Advances*, 4, 46340. doi:
811 10.1039/c4ra08362h

812 Brooke, M., Cole, E., Dale, J., Prasad, A., Quach, H., Bau, B., Nowacek, D., & Bhatt, E. (2016). An
813 ocean sensor for measuring the seawater electrochemical response of 8 metals referenced to zinc,
814 for determining ocean pH. *9th International Conference on Sensing Technology (ICST)*, Auckland
815 (NZ), 8-11 December 2015, 147-150. doi: 10.1109/ICSensT.2015.7438381

816 Buck, R.P., Rondinini, S., Covington, A.K., Baucke, F.G.K., Brett, C.M.A., Camões, M.F., Milton,
817 M.J.T., Mussini, T., Naumann, R., Pratt, K.W., & Spitzer, P. (2002). Measurement of pH. Definition,
818 standards, and procedures. *Pure Appl. Chem.*, 74(11), 2169–2200. <http://hdl.handle.net/1808/8412>

819 Bushinsky, S.M., Takeshita, Y., & Williams, N.L. (2019). Observing Changes in Ocean Carbonate
820 Chemistry: Our Autonomous Future. *Current Climate Change Reports*, 5(3), 207-220. doi:
821 10.1007/s40641-019-00129-8

822 Byrne, R.H. (2014). Measuring Ocean Acidification: New Technology for a New Era of Ocean
823 Chemistry. *Environmental Science and Technology*, 48(10), 5352-5360. doi: 10.1021/es405819p

824 Cachet-Vivier, C., Tribollet, B., Vivier, V. (2010). Cavity microelectrode for studying manganese
825 dioxide powder as pH sensor. *Talanta*, 82(2), 555–559. doi: 10.1016/j.talanta.2010.05.006

826 Chen, X.M., Wu, G.H., Jiang, Y.Q., Wang, Y.R., & Chen, X. (2011). Graphene and graphene-based
827 nanomaterials: the promising materials for bright future of electroanalytical chemistry. *Analyst*,
828 136(22), 4631-40. doi: 10.1039/c1an15661f

829 Cheng, Z., Li, Q., Li, Z., Zhou, Q., & Fang, Y. (2010). Suspended Graphene Sensors with Improved
830 Signal and Reduced Noise. *Nano Letters*, 10, 1864–1868. doi: 10.1021/nl100633g

831 Chien, Y.-S., Tsai, W.-L., Lee, I.-C., Chou, J.-C., & Cheng, H.-C. (2012). Novel Ph Sensor Of Egfets
832 With Laser-Irradiated Carbon-Nanotube Network. *IEEE Electron Device Letters*, 33(11), 1622-
833 1624. doi: 10.1109/LED.2012.2213794

834 Chinnathambi, S., & Euverink, G.J.W. (2018). Polyaniline functionalized electrochemically reduced
835 graphene oxide chemiresistive sensor to monitor the pH in real time during microbial
836 fermentations. *Sensors and Actuators B: Chemical*, 264, 38–44. doi: 10.1016/j.snb.2018.02.087

837 Choi, J.-S, Savagatrup, S., Kim, Y., Lang, J.H., & Swager, T.M. (2019). Precision pH sensor based on
838 WO₃ nanofiber-polymer composites and different amplification. *ACS Sensors*, 4(10), 2593-2598.
839 doi: 10.1021/acssensors.9b01579

840 Choi, S., Park, I., Hao, Z., Holman, H.-Y. N., & Pisano, A.P. (2012). Quantitative studies of long-term
841 stable, top-down fabricated silicon nanowire pH sensors. *Applied Physics A*, 107, 421–428. doi:
842 10.1007/s00339-011-6754-9

843 Cisternas, R., Kahlert, H., Scholz, F., & Wulff, H. (2015). Direct contact tungsten bronze electrodes for
844 calibration-free potentiometric pH measurements. *Electrochemistry Communications*, 60, 17-20.
845 doi: 10.1016/j.elecom.2015.07.017

846 Cisternas, R., Ballesteros, L., Valenzuela, M.L., Kahlert, H., & Scholz, F. (2017). Decreasing the time
847 response of calibration-free pH sensors based on tungsten bronze nanocrystals. *Journal of*
848 *Electroanalytical Chemistry*, 801, 315–318. doi: 10.1016/j.jelechem.2017.08.005

849 Clarke, J.S., Achterberg, E.P., Rérolle, V.M.C., Abi Kaed Bey, S., Floquet, C.F.A., Mowlem, M.C.
850 (2015). Characterisation and deployment of an immobilised pH sensor spot towards surface ocean
851 pH measurements. *Analytica Chimica Acta*, 897, 69–80. doi: 10.1016/j.aca.2015.09.026

852 Cleary, J., McCaul, M., Diamond, D., García, M.B.G., Díez, C., Rovira, C., Challiss, M., Lassoued, Y.,
853 Ribotti, A., Sáez, J. (2014). COMMON SENSE: Cost-effective sensors, interoperable with
854 international existing ocean observing systems, to meet EU policies requirements. *2014 IEEE*
855 *Sensor Systems for a Changing Ocean (SSCO 2014)*, 1-7, doi: 10.1109/SSCO.2014.7000384

856 Crespo, G.A., Gugsa, D., Macho, S., & Rius, F.X. (2009). Solid-contact pH-selective electrode using
857 multi-walled carbon nanotubes. *Analytical and Bioanalytical Chemistry*, 395, 2371-2376. doi:
858 10.1007/s00216-009-3127-8

859 Cuartero, M., Pankratova, N., Cherubini, T., Crespo, G., Massa, F., Confalonieri, F., & Bakker, E.
860 (2017). In Situ Detection of Species Relevant to the Carbon Cycle in Seawater with Submersible
861 Potentiometric Probes. *Environmental Science & Technology Letters*, 4. doi:
862 10.1021/acs.estlett.7b00388

863 Culebras, M., Gómez, C.M., & Cantarero, A. (2014). Review on Polymers for Thermoelectric
864 Applications. *Materials*, 7(9), 6701-6732. doi: 10.3390/ma7096701

865 Cullison Gray, S.E., DeGrandpre, M.D., Moore, T.S., Martz, T.R., Friederich, G.E., & Johnson, K.S.
866 (2011). Applications of in situ pH measurements for inorganic carbon calculations. *Marine*
867 *Chemistry*, 125(1-4), 82–90. doi: 10.1016/j.marchem.2011.02.005

868 Dai, C., Chan, C.-W.I., Barrow, W., Smith, A., Song, P., Potier, F., Wadhawan, J.D., Fisher, A.C., &
869 Lawrence, N.S. (2016). A Route to Unbuffered pH Monitoring: A Novel Electrochemical Approach.
870 *Electrochimica Acta*, 190, 879-886. doi: 10.1016/j.electacta.2016.01.004

871 Fu, W., Nef, C., Knopfmacher, O., Tarasov, A., Weiss, M., Calame, M., & Schönenberger, C. (2011).
872 Graphene Transistors Are Insensitive to pH Changes in Solution. *Nano Letters*, 11(9), 3597–3600.
873 doi: 10.1021/nl201332c

874 Fulati, A., Usman Ali, S.M., Riaz, M., Amin, G., Nur, O., & Willander, M. (2009). Miniaturized pH
875 Sensors Based on Zinc Oxide Nanotubes/Nanorods. *Sensors*, 9(11), 8911-8923. doi:
876 10.3390/s91108911

877 Gambi, M.C., Musco, L., Giangrande, A., Badalamenti, F., Micheli, F., Kroeker, K. (2016). Distribution
878 and functional traits of polychaetes in a CO₂ vent system: winners and losers among closely
879 related species. *Marine Ecology Progress Series*, 550, 121-134. doi: 10.3354/meps11727

880 Gao, W., & Song, J. (2009). Polyaniline Film Based Amperometric pH Sensor Using A Novel
881 Electrochemical Measurement System. *Electroanalysis*, 21(8), 973-978. doi:
882 10.1002/elan.200804500

883 Gill, E., Arshak, A., Arshak, K., & Korostynska, O. (2008). Conductometric pH sensor based on novel
884 conducting polymer composite thick films. *Proceedings of the 2008 31st International Spring*
885 *Seminar on Electronics Technology*, 478–483. doi: 10.1109/ISSE.2008.5276613

886 Glab, S., Hulanicki, A., Edwall, G., & Ingman F. (1989). Metal-Metal Oxide and Metal Oxide
887 Electrodes as pH Sensors. *Critical Reviews in Analytical Chemistry*, 21(1), 29-47. doi:
888 10.1080/10408348908048815

889 González Durán, E., Cuaya, M.P., Gutiérrez, M.V. & Ancona León, J. (2018). Effects of Temperature
890 and pH on the Oxidative Stress of Benthic Marine Invertebrates. *Biology Bulletin*, 45, 610–616.
891 doi: 10.1134/S1062359018660019

892 Gou, P., Kraut, N.D., Feigel, I.M., Bai, H., Morgan, G.J., Chen, Y., Tang, Y., Bocan, K., Stachel, J.,
893 Berger, L., Mickle, M., Sejdic, E., & Star, A., (2014). Carbon Nanotube Chemiresistor for Wireless
894 pH Sensing. *Scientific Reports*, 4, 4468. doi: 10.1038/srep04468

895 Grozdanov, A., Petrovski, A., Paunovic, P., Dimitrov, T.A., & Avella M. (2018). MWCNT/Polyaniline
896 nanocomposites used for pH nanosensors of marine waters. In M. Cocca, E. Di Pace, M. Errico,
897 G. Gentile, A. Montarsolo, R. Mossotti (Eds.), *Proceedings of the International Conference on*
898 *Microplastic Pollution in the Mediterranean Sea*, (pp. 231-238). Springer International Publishing.
899 doi: 10.1007/978-3-319-71279-6_32

900 Grozdanov, A., Petrovski, A., Avella, M., Paunovic, P., Errico, E.M., Avolio, R., Gentile, G., De Falco,
901 F., & Dimitrov, T. A. (2019). Spectroscopic study of nanocomposite based on PANI and Carbon
902 nanostructures for pH sensors. *Bulgarian Chemical Communications*, 51(D), 36-41.

903 Gupta, N., Sharma, S., Mir, I.A., & Kumar, D. (2006). Advances in sensors based on conducting
904 polymers. *Journal of Scientific and Industrial Research*, 65(7), 549-557.
905 <http://nopr.niscair.res.in/handle/123456789/4862>

906 Hayat, A., & Marty, J.L. (2014). Disposable screen printed electrochemical sensors: tools for
907 environmental monitoring. *Sensors*, 14(6), 10432-53. doi: 10.3390/s140610432

908 Heller, I., Chatoor, S., Mannik, J., Zevenbergen, M.A.G., Dekker, C., & Lemay, S.G. (2010). Influence
909 of Electrolyte Composition on Liquid-Gated Carbon Nanotube and Graphene Transistors. *Journal*
910 *of the American Chemical Society*, 132(48), 17149-17156. doi: 10.1021/ja104850n

911 Hu, J., Ho, K.T., Zou, X.U., Smyrl, W.H., Stein, A., & Bühlmann, P. (2015). All-Solid-State Reference
912 Electrodes Based on Colloid-Imprinted Mesoporous Carbon and their Application in Disposable
913 Paper-based Potentiometric Sensing Devices. *Analytical Chemistry*, 87(5), 2981–2987. doi:
914 10.1021/ac504556s

915 Huang, W.S., Humphrey, B.D., & MacDiarmid, A.G. (1986). Polyaniline, a novel conducting polymer.
916 Morphology and chemistry of its oxidation and reduction in aqueous electrolytes. *J. Chem. Soc.,*
917 *Faraday Trans. 1: Physical Chemistry in Condensed Phases*, 82(8), 2385-2400. doi:
918 10.1039/F19868202385

919 Jamal, M., Razeeb, K.M., Shao, H., Islam, J., Akhter, I., Furukawa, H., & Khosla, A. (2019).
920 Development of Tungsten Oxide Nanoparticle Modified Carbon Fibre Cloth as Flexible pH Sensor.
921 *Scientific Reports*, 9(1), Article number 4659. doi: 10.1038/s41598-019-41331-w

922 Jang, H., & Lee, J. (2020). Iridium oxide fabrication and application: A review. *Journal of Energy*
923 *Chemistry*, 46, 152-172. doi: 10.1016/j.jechem.2019.10.026

924 Jin, Q. & Kirk, M.F. (2018). pH as a Primary Control in Environmental Microbiology: 1.
925 Thermodynamic Perspective. *Frontiers in Environmental Science*, 6:21. doi:
926 10.3389/fenvs.2018.00021

927 Johnson, K.S., Jannasch, H.W., Coletti, L.J., Elrod, V.A., Martz, T.R., Takeshita, Y., Carlson, R.J., &
928 Connery, J.C. (2016). Deep-Sea DuraFET: A Pressure Tolerant pH Sensor Designed for Global
929 Sensor Networks. *Analytical Chemistry*, 88(6), 3249-3256. doi: 10.1021/acs.analchem.5b04653

930 Jović, M., Hidalgo-Acosta, J.C., Lesch, A., Costa Bassetto, V., Smirnov, E., Cortés-Salazar, F., &
931 Girault, H.H. (2018). Large-scale layer-by-layer inkjet printing of flexible iridium-oxide based pH
932 Sensors. *Journal of Electroanalytical Chemistry*, 819, 384–390. doi:
933 10.1016/j.jelechem.2017.11.032

934 Jung, M.W., Myung, S., Song, W., Kang, M.A., Kim, S.H., Yang, C.S., Lee, S.S., Lim, J., Park, C.Y.,
935 Lee, J.O., & An, K.S. (2014). Novel fabrication of flexible graphene-based chemical sensors with

936 heaters using soft lithographic patterning method. *ACS Applied Materials & Interfaces*, 6(16),
937 13319-13323. doi: 10.1021/am502281t

938 Khan, M.I., Mukherjee, K., Shoukat, R. & Dong, H. (2017). A review on pH sensitive materials for
939 sensors and detection methods. *Microsystem Technologies*, 23, 4391–4404. doi: 10.1007/s00542-
940 017-3495-5

941 Kim, D.-M., Cho, S.J., Cho, C.-H., Kim, K.B., Kim, M.-Y., & Shim, Y.-B. (2016). Disposable all-solid-
942 state pH and glucose sensors based on conductive Polymer covered hierarchical AuZn oxide.
943 *Biosensors and Bioelectronics*, 79, 165–172. doi: 10.1016/j.bios.2015.12.002

944 Kim, K., Park, C., Rim, T., Meyyappan, M., & Lee, J.-S. (2014). Electrical and pH Sensing
945 Characteristics of Si Nanowire-Based Suspended FET Biosensors. *Proceedings of the 14th IEEE
946 International Conference on Nanotechnology Toronto, Canada, August 18-21*

947 Kim, T.Y., & Yang, S. (2014). Fabrication method and characterization of electrodeposited and heat-
948 treated iridium oxide films for pH sensing. *Sensors and Actuators B: Chemical*, 196, 31-38. doi:
949 10.1016/j.snb.2014.02.004

950 King, D.W., & Kester, D.R. (1989). Determination of seawater pH from 1.5 to 8.5 using colorimetric
951 indicator. *Marine Chemistry*, 26(1), 5-20. doi: 10.1016/0304-4203(89)90061-3

952 Kinoshita, E., Ingman, F., Edwalla, G., Thulina, S., & Głąb, S. (1986). Polycrystalline and
953 monocrystalline antimony, iridium and palladium as electrode material for pH-sensing electrodes.
954 *Talanta*, 33(2), 125-134. doi: 10.1016/0039-9140(86)80028-5

955 Knopfmacher, O., Tarasov, A., Fu, W., Wipf, M., Niesen, B., Calame, M., & Schönenberger, C. (2010).
956 Nernst Limit in Dual-Gated Si-Nanowire FET Sensors. *Nano Letters*, 10(6), 2268–2274. doi:
957 10.1021/nl100892y

958 Koncki, R., & Mascini, M. (1997). Screen-printed ruthenium dioxide electrodes for pH measurements.
959 *Analytica Chimica Acta*, 351(1–3), 143–149. doi: 10.1016/S0003-2670(97)00367-X

960 Korostynska, O., Arshak, K., Gill, E., & Arshak, A. (2007). Review on state-of-the-art in Polymer
961 Based pH sensors. *Sensors*, 7(12), 3027-3042. doi: 10.3390/s7123027

962 Kroeker, K.J., Kordas, R., Crim, R., Hendriks, I.E., Ramajo, L., Singh, G.S., Duarte, C.D., & Gattuso,
963 J.-P. (2013). Impacts of ocean acidification on marine organisms: quantifying sensitivities and
964 interaction with warming. *Global Change Biology*, 19(6), 1884-1896. doi: 10.1111/gcb.12179

965 Kumar, A., Kumar, N., Aniley, A.A., Fernandez, R.E., & Bhansali, S. (2019). Hydrothermal growth of
966 zinc oxide (ZnO) nanorods (NRs) on screen printed IDEs for ph measurement application. *Journal
967 of the Electrochemical Society*, 166, B3264-B3270. doi: 10.1149/2.0431909jes

968 Kumar, N., Sutradhar, M., Kumar, J., & Panda, S. (2017). Role of deposition and annealing of the top
969 gate dielectric in a-IGZO TFT-based dual-gate ion-sensitive field-effect transistors. *Semiconductor
970 Science and Technology*, 32, 035013. doi: 10.1088/1361-6641/aa5584

971 Kuo, L.-M., Chou, Y.-C., Chen, K.-N., Lu, C.-C., Chao, S. (2014). A precise pH microsensor using RF-
972 sputtering IrO₂ and Ta₂O₅ films on Pt-electrode. *Sensors and Actuators B: Chemical*, 193, 687-
973 691. doi: 10.1016/j.snb.2013.11.109

974 Kurihara, H., 2008. Effects of CO₂-driven ocean acidification on the early developmental stages of
975 invertebrates. *Marine Ecology Progress Series*, 373, 275-284. doi: 10.3354/meps07802

976 Lacoue-Labarthe, T., Nunes, P.A.L.D., Ziveri, P., Cinar, M., Gazeau, F., Hilmi, N., Moschella, P., Safa,
977 A., Sauzade, D., & Turley, C. (2016). Impacts of ocean acidification in a warming Mediterranean
978 Sea: An overview. *Regional Studies in Marine Science*, 5, 1-11. doi: 10.1016/j.rsma.2015.12.005

979 Lai, C.-Z., DeGrandpre, M.D., & Darlington, R.C. (2018). Autonomous Optofluidic Chemical Analyzers
980 for Marine Applications: Insights from the Submersible Autonomous Moored Instruments (SAMI)
981 for pH and pCO₂. *Frontiers in Marine Science*, 4, 438. doi: 10.3389/fmars.2017.00438

982 Lakard, B., Segut, O., Lakard, S., Herlem, G., & Gharbi, T. (2007). Potentiometric miniaturized pH
983 sensors based on polypyrrole films. *Sensors and Actuators B: Chemical*, 122, 101-108. doi:
984 10.1016/j.snb.2006.04.112

985 Lee, D., & Cui, T. (2010). Low-cost, transparent, and flexible single-walled carbon nanotube
986 nanocomposite based ion-sensitive field-effect transistors for pH/glucose sensing. *Biosensors and*
987 *Bioelectronics*, 25(10), 2259–2264. doi: 10.1016/j.bios.2010.03.003

988 Lei, K.F., Lee, K.-F., & Yang, S.-I (2012). Fabrication of carbon nanotube-based pH sensor for paper-
989 based microfluidics. *Microelectronic Engineering*, 100, 1–5. doi: 10.1016/j.mee.2012.07.113

990 Lenar, N., Paczosa-Bator, B., & Piech, R. (2019). Ruthenium dioxide nanoparticles as a high-capacity
991 transducer in solid-contact polymer membrane-based pH-selective electrodes. *Microchimica Acta*,
992 186(12), Article n. 777. doi: 10.1007/s00604-019-3830-x

993 Li, H.-H., Dai, W.-S., Chou, J.-C., & Cheng, H.-C. (2012). An Extended-Gate Field-Effect Transistor
994 With Low-Temperature Hydrothermally Synthesized SnO₂ Nanorods as pH Sensor. *IEEE Electron*
995 *Device Letters*, 33(10), 1495-1497. doi: 10.1109/LED.2012.2210274

996 Li, Q., Li, H., Zhang, J., & Xu, Z. (2011). A novel pH potentiometric sensor based on electrochemically
997 synthesized polybisphenol A films at an ITO electrode. *Sensors and Actuators B: Chemical*, 155,
998 730–736. doi: 10.1016/j.snb.2011.01.038

999 Li, X., Cai, W., An, J., Kim, S., Nah, J., Yang, D., Piner, R., Velamakanni, A., Jung, I., Tutuc, E.,
1000 Banerjee, S.K., Colombo, L., & Ruoff, R.S. (2009). Large-area synthesis of high-quality and
1001 uniform graphene films on copper foils. *Science*, 324(5932), 1312-1314. doi:
1002 10.1126/science.1171245

1003 Li, Y., Mao, Y., Xiao, C., Xu, X., & Li, X. (2020). Flexible pH sensor based on a conductive PANI
1004 membrane for pH monitoring. *RSC Advances*, 10, 21-28. doi: 10.1039/C9RA09188B

- 1005 Lin, J.-C., Huang, B.-R., & Yang, Y.-K. (2013). IGZO nanoparticle-modified silicon nanowires as
1006 extended-gate field-effect transistor pH sensors. *Sensors and Actuators B: Chemical*, 184, 27–32.
1007 doi: 10.1016/j.snb.2013.04.060
- 1008 Liu, M., Ma, Y., Su, L., Chou, K.-C., & Hou, X. (2016). A titanium nitride nanotube array for
1009 potentiometric sensing of pH. *Analyst*, 141(5), 1693-1699. doi: 10.1039/c5an02675j
- 1010 Liu, Y., & Cui, T. (2007). Ion-sensitive field-effect transistor based pH sensors using nano self-
1011 assembled polyelectrolyte/nanoparticle multilayer films. *Sensors and Actuators B: Chemical*, 123,
1012 148–152. doi: 10.1016/j.snb.2006.08.006
- 1013 Loh, K.J., Lynch, J.P., & Kotov, N.A. (2007). Passive wireless strain and pH sensing using carbon
1014 nanotube-gold nanocomposite thin films. In M. Tomizuka, C.-B. Yun, V. Giurgiutiu (Eds.), *Sensors*
1015 *and Smart Structures Technologies for Civil, Mechanical, and Aerospace Systems, Processing of*
1016 *SPIE*, 6529, 652919-652931. doi: 10.1117/12.715826
- 1017 Lonsdale, W., Wajrak, M., & Alameh, K. (2018). Manufacture and application of RuO₂ solid-state
1018 metal-oxide pH sensor to common beverages. *Talanta*, 180, 277-281. doi:
1019 10.1016/j.talanta.2017.12.070
- 1020 Maily-Giacchetti, B., Hsu, A., Wang, H., Vinciguerra, V., Pappalardo, F., Occhipinti, L., Guidetti, E.,
1021 Coffa, S., Kong, J., & Palacios, T. (2013). pH sensing properties of graphene solution-gated field-
1022 effect transistors. *Journal of Applied Physics*, 114, 084505. doi: 10.1063/1.4819219
- 1023 Manjakkal, L., Cvejic, K., Kulawik, J., Zaraska, K., Szwagierczak, D., & Socha, R.P. (2014).
1024 Fabrication of thick film sensitive RuO₂-TiO₂ and Ag/AgCl/KCl reference electrodes and their
1025 application for pH measurements. *Sensors and Actuators B: Chemical*, 204, 57–67. doi:
1026 10.1016/j.snb.2014.07.067
- 1027 Manjakkal, L., Synkiewicz, B., Zaraska, K., Cvejic, K., Kulawik, J., & Szwagierczak, D. (2016).
1028 Development and characterization of miniaturized LTCC pH sensors with RuO₂ based sensing
1029 electrodes. *Sensors and Actuators B: Chemical*, 223, 641–649. doi: 10.1016/j.snb.2015.09.135
- 1030 Marion, G. M., Millero, F. Camões, M.F., Spitzer, P., Feistel, R., & Chen, C.T.A. (2011). pH of
1031 seawater. *Marine Chemistry*, 126, 89-96. doi: 10.1016/j.marchem.2011.04.002
- 1032 Martin, A., & Escarpa, A. (2014). Graphene: The cutting-edge interaction between chemistry and
1033 electrochemistry. *TrAC Trends in Analytical Chemistry*, 56, 13-26. doi: 10.1016/j.trac.2013.12.008
- 1034 Martz, T., McLaughlin, K., Weisberg, S.B. (2015). Best Practices for autonomous measurement of
1035 seawater pH with the Honeywell Durafet pH sensor. *Technical Report 861. California Current*
1036 *Acidification Network. Santa Barbara, CA.*
1037 [http://ftp.sccwrp.org/pub/download/DOCUMENTS/TechnicalReports/861_CCAN_Durafet_Best_Pr](http://ftp.sccwrp.org/pub/download/DOCUMENTS/TechnicalReports/861_CCAN_Durafet_Best_Practices_Manual.pdf)
1038 [actices_Manual.pdf](http://ftp.sccwrp.org/pub/download/DOCUMENTS/TechnicalReports/861_CCAN_Durafet_Best_Practices_Manual.pdf)
- 1039 McLaughlin, K., Dickson, A., Weisberg, S.B., Coale, K., Elrod, V., Hunter, C., Johnson, K.S., Kram, S.,
1040 Kudela, R., Martz, T., Negrey, K., Passow, U., Shaughnessy, F., Smith, J.E., Tadesse, D.,

1041 Washburn, L., & Weis, K.R. (2017a). An evaluation of ISFET sensors for coastal pH monitoring
1042 applications. *Regional Studies in Marine Science*, 12, 11-18. doi: 10.1016/j.rsma.2017.02.008

1043 McLaughlin, K., Nezhlin, N.P., Weisberg, S.B., Dickson, A.G., Booth, J.A., Cash, C.L., Feit, A., Gully,
1044 J.R., Johnson, S., Latker, A., Mengel, M.J., Robertson, G.L., Steele, A., & Terriquez, L. (2017b).
1045 An evaluation of potentiometric pH sensors in coastal monitoring applications. *Limnology and*
1046 *Oceanography: Methods*, 15, 679-689. doi: 10.1002/lom3.10191

1047 Michalska, A. (2012). All-Solid-State Ion Selective and All-Solid-State Reference Electrodes.
1048 *Electroanalysis*, 24, 1253–1265. doi: 10.1002/elan.201200059

1049 Millero, F.J., DiTrollo, B., Suarez, A.F., & Lando, G. (2009). Spectroscopic measurements of the pH in
1050 NaCl brines. *Geochimica Cosmochimica Acta*, 73, 3109–3114. doi: 10.1016/j.gca.2009.01.037

1051 Moya, A., Pol, R., Martínez-Cuadrado, A., Villa, R., Gabriel, G., & Baeza, M. (2019). Stable Full-Inkjet-
1052 Printed Solid-State Ag/AgCl Reference Electrode. *Analytical Chemistry*, 91(24), 15539-15546. doi:
1053 10.1021/acs.analchem.9b03441

1054 Novoselov, K.S., Falko, V.I., Colombo, L., Gellert, P.R., Schwab, M.G., & Kim, K. (2012). A roadmap
1055 for graphene. *Nature*, 490(7419), 192-200. doi: 10.1038/nature11458

1056 Ohno, Y., Maehashi, K., Yamashiro, Y., & Matsumoto, K. (2009). Electrolyte-Gated Graphene Field-
1057 Effect Transistors for Detecting pH and Protein Adsorption. *Nano Letters*, 9(9), 3318-3322. doi:
1058 10.1021/nl901596m

1059 Ohno, Y., Maehashi, K., & Matsumoto, K. (2010). Chemical and biological sensing applications based
1060 on graphene field-effect transistors. *Biosensors and Bioelectronics*, 26, 1727–1730. doi:
1061 10.1016/j.bios.2010.08.001

1062 Okazaki, R.R., Sutton, A.J., Feely, R.A., Dickson, A.G., Alin, S.R., Sabine, C.L., Bunje, P.M.E., &
1063 Virmani, J.I. (2017). Evaluation of marine pH sensors under controlled and natural conditions for
1064 the Wendy Schmidt Ocean Health XPRIZE. *Limnology and Oceanography: Methods*, 15, 586–600.
1065 doi: 10.1002/lom3.10189

1066 Oueiny, C., Berlioz, S., & Perrin, F.-J. (2014). Carbon nanotube–polyaniline composites. *Progress in*
1067 *Polymer Science*, 39(4), 707–748. doi: 10.1016/j.progpolymsci.2013.08.00

1068 Pan, Y., Sun, Z., He, H., Li, Y., You, L., & Zheng, H. (2018). An improved method of preparing iridium
1069 oxide electrode based on carbonate-melt oxidation mechanism. *Sensors and Actuators B:*
1070 *Chemical*, 261, 316-324. doi: 10.1016/j.snb.2018.01.069

1071 Pandey, P.C., & Singh, G. (2001). Tetraphenylborate doped polyaniline based novel pH sensor and
1072 solid-state urea biosensor. *Talanta*, 55(4), 773–782. doi: 10.1016/S0039-9140(01)00505-7

1073 Parizi, K.B., Yeh, A.J., Poon, A.S.Y., & Wong, H.S.P. (2012). Exceeding Nernst limit (59mV/pH):
1074 CMOS-based pH sensor for autonomous applications. *2012 International Electron Devices*
1075 *Meeting*, 24.7.1 - 24.7.4. doi: 10.1109/IEDM.2012.6479098

- 1076 Park, H.J., Yoon, J.H., Lee, K.G., & Choi, B.G. (2019). Potentiometric performance of flexible pH
 1077 sensor based on polyaniline nanofiber arrays. *Nano Convergence*, 6(1), Article n. 9. doi:
 1078 10.1186/s40580-019-0179-0
- 1079 Park, I., Li, Z., Pisano, A.P., & Williams, R.S. (2010). Top-down fabricated silicon nanowire sensors
 1080 for real-time chemical detection. *Nanotechnology*, 1, 015501. doi: 10.1088/0957-4484/21/1/015501
- 1081 Patil, S., Ghadi, H., Ramgir, N., Adhikari, A., & Rao, V.R. (2019). Monitoring soil pH variation using
 1082 Polyaniline/SU-8 composite film based conductometric microsensor. *Sensors and Actuators B:
 1083 Chemical*, 286, 583-590. doi: 10.1016/j.snb.2019.02.016
- 1084 Persaud, K.C., & Pelosi, P. (1985). An approach to an artificial nose. *Transactions - American Society
 1085 for Artificial Internal Organs*, 31, 297–300.
- 1086 Pfattner, R., Foudeh, A.M., Chen, S., Niu, W., Matthews, J.R., He, M., & Bao, Z. (2019). Dual-Gate
 1087 Organic Field-Effect Transistor for pH Sensors with Tunable Sensitivity. *Advanced Electronic
 1088 Materials*, 5(1), Article n. 1800381. doi: 10.1002/aelm.201800381
- 1089 Poma, N., Vivaldi, F., Bonini, A., Carbonaro, N., Di Rienzo, F., Melai, B., Kirchhain, A., Salvo, P.,
 1090 Tognetti, A., & Di Francesco, F. (2019). Remote monitoring of seawater temperature and pH by
 1091 low cost sensors. *Microchemical Journal*, 148, 248-252. doi: 10.1016/j.microc.2019.05.001
- 1092 Pyo, J.-Y., & Cho, W.-J. (2017). High-performance SEGISFET pH Sensor using the structure of
 1093 double-gate a-IGZO TFTs with engineered gate oxides. *Semiconductor Science and Technology*,
 1094 32(3), Article N. 035015. doi: 10.1088/1361-6641/aa584b
- 1095 Qin, Y., Kwon, H.-J., Subrahmanyam, A., Howlader, M.M.R., Selvaganapathy, P.R., Adronov, A., &
 1096 Deen, M.J. (2016). Inkjet-printed bifunctional carbon nanotubes for pH sensing. *Materials Letters*,
 1097 176, 68–70. doi: 10.1016/j.matlet.2016.04.048
- 1098 Radu, A., Anastasova, S., Fay, C., Diamond, D., Bobacka, J. & Lewenstam, A. (2010). Low cost,
 1099 calibration-free sensors for in situ determination of natural water pollution. *SENSORS, 2010 IEEE*,
 1100 1487-1490. doi: 10.1109/ICSENS.2010.5690357
- 1101 Rahimi, R., Ochoa, M., Parupudi, T., Zhao, X., Yazdi, I.K., Dokmeci, M.R., Tamayol, A.,
 1102 Khademhosseini, A., & Ziaie, B. (2016). A low-cost flexible pH sensor array for wound
 1103 assessment. *Sensors and Actuators B: Chemical*, 229, 609–617. doi: 10.1016/j.snb.2015.12.082
- 1104 Ramanathan, T., Abdala, A.A., Stankovich, S., Dikin, D.A., Herrera-Alonso, M., Piner, R.D., Adamson,
 1105 D.H., Schniepp, H.C., Chen, X., Ruoff, R.S., Nguyen, S.T., Aksay, I.A., Prud'Homme, R.K., &
 1106 Brinson, LC. (2008). Functionalized graphene sheets for polymer nanocomposites. *Nature
 1107 Nanotechnology*, 3(6), 327-331. doi: 10.1038/nnano.2008.96
- 1108 Rérolle, V.M.C., Floquet, C.F.A., Mowlem, M.C., Connelly, D.P., Achterberg, E.P., & Bellerby,
 1109 R.R.G.J. (2012). Seawater-pH measurements for ocean-acidification observations. *TrAC Trends in
 1110 Analytical Chemistry*, 40, 146-157. doi: 10.1016/j.trac.2012.07.016

- 1111 Rérolle, V.M.C., Achterberg, E.P., Ribas-Ribas, M., Kitidis, V., Brown, I., Bakker, D.C.E., Lee, G.A., &
1112 Mowlem, M.C. (2018). High Resolution pH Measurements Using a Lab-on-Chip Sensor in Surface
1113 Waters of Northwest European Shelf Seas. *Sensors*, 18(8), 2622. doi: 10.3390/s18082622
- 1114 Ribotti, A., Magni, P., Borghini, M., Schroeder, K., Barton, J., McCaul, M., Diamond, D., (2015), New
1115 cost-effective, interoperable sensors tested on existing ocean observing platforms in application of
1116 European directives: The COMMON SENSE European project. *Proceedings of the IEEE OCEANS*
1117 *2015 Conference*, 1-9. doi: 10.1109/OCEANS-Genova.2015.7271340
- 1118 Saba, G.K., Wright-Fairbanks, E., Chen, B., Cai, W.-J., Barnard, A.H., Jones, C.P., Branham, C.W.,
1119 Wang, K., & Miles, T. (2019). The Development and Validation of a Profiling Glider Deep ISFET-
1120 Based pH Sensor for High Resolution Observations of Coastal and Ocean Acidification. *Frontiers*
1121 *in Marine Science*, 6, Article n. 664. doi: 10.3389/fmars.2019.00664
- 1122 Sadig, H.R., Cheng, L., & Xiang, T. (2018). Using sol-gel supported by novel economic and
1123 environment-friendly spray-coating in the fabrication of nanostructure tri-system metal oxide-based
1124 pH sensor applications. *Journal of Electroanalytical Chemistry*, 827, 93-102. doi:
1125 10.1016/j.jelechem.2018.09.017
- 1126 Salaün, A-C., Pichon, L., & Wenga, G. (2014). Polysilicon nanowires FET as highly-sensitive pH-
1127 sensor: modeling and measurements. *Procedia Engineering*, 87, 911 – 914. doi:
1128 10.1016/j.proeng.2014.11.303
- 1129 Salavagione, H.J., Diez-Pascual, A.M., Lazaro, E., Vera, S., & Gomez-Fatou, M.A. (2014). Chemical
1130 sensors based on polymer composites with carbon nanotubes and graphene: the role of the
1131 polymer. *Journal of Materials Chemistry A*, 2, 14289. doi: 10.1039/C4TA02159B
- 1132 Salvo, P., Calisi, N., Melai, B., Cortigiani, B., Mannini, M., Caneschi, A., Lorenzetti, G., Paoletti, C.,
1133 Lomonaco, T., Paolicchi, A., Scataglini, I., Dini, V., Romanelli, M., Fuoco, R., & Di Francesco, F.
1134 (2017). Temperature and pH sensors based on graphenic materials. *Biosensors and*
1135 *Bioelectronics*, 91, 870-877. doi: 10.1016/j.bios.2017.01.062
- 1136 Santos, L., Neto, J.P., Crespo, A., Nunes, D., Costa, N., Fonseca, I.M., Barquinha, P., Pereira, L.,
1137 Silva, J., Martins, R., & Fortunato, E. (2014). WO₃ nanoparticle-based conformable pH sensor.
1138 *ACS Applied Materials and Interfaces*, 6(15), 12226-12234. doi: 10.1021/am501724h
- 1139 Segut, O., Lakard, B., Herlem, G., Rauch, J.-Y., Jeannot, J.-C., Robert, L., & Fahys, B. (2007).
1140 Development of miniaturized pH biosensors based on electrosynthesized polymer films. *Analytica*
1141 *Chimica Acta*, 597(2), 313-321. doi: 10.1016/j.aca.2007.06.053
- 1142 Sha, R., Komori, K., & Badhulika, S. (2017). Amperometric pH Sensor Based on Graphene-
1143 Polyaniline Composite. *IEEE Sensors Journal*, 17(16), Article n. 7959556, 5038-5043. doi:
1144 10.1109/JSEN.2017.2720634
- 1145 Sharma, B.K., & Ahn, J.-H. (2013). Graphene based field effect transistors: Efforts made towards
1146 flexible electronics. *Solid-State Electronics*, 89, 177–195. doi: 10.1016/j.sse.2013.08.007

- 1147 Shirale, D.J., Bangar, M.A., Chen, W., Myung, N.V., & Mulchandani, A. (2010). Effect of aspect ratio
 1148 (length:diameter) on a single polypyrrole nanowire FET device. *Journal of Physical Chemistry C*,
 1149 114, 13375–13380. doi: 10.1021/jp104377e
- 1150 Singh, K., Lou, B.-S., Her, J.-L., Pang, S.-T., & Pan, T.-M. (2019). Super Nernstian pH response and
 1151 enzyme-free detection of glucose using sol-gel derived RuO_x on PET flexible-based extended-gate
 1152 field-effect transistor. *Sensors and Actuators B: Chemical*, 298, Article n.126837. doi:
 1153 10.1016/j.snb.2019.126837
- 1154 Sohn, I.-Y., Kim, D.-J., Jung, J.-H., Yoon, O.J., Thanh, T.N., Quang, T.T., & Lee, N.E. (2013). pH
 1155 sensing characteristics and biosensing application of solution-gated reduced graphene oxide field-
 1156 effect transistors. *Biosensors and Bioelectronics*, 45, 70–76. doi: 10.1016/j.bios.2013.01.051
- 1157 Somero, G.N., Beers, J.M., Chan, F., Hill, T.M., Klinger, T., & Litvin, S.Y. (2016). What changes in the
 1158 carbonate system, oxygen, and temperature portend for the Northeastern Pacific Ocean: A
 1159 physiological perspective. *BioScience*, 66, 14–26. doi: 10.1093/biosci/biv162
- 1160 Sophocleous, M., & Atkinson, J.K. (2017). A review of screen-printed silver/silver chloride (Ag/AgCl)
 1161 reference electrodes potentially suitable for environmental potentiometric sensors. *Sensors and*
 1162 *Actuators A: Physical*, 267, 106-120. doi: 10.1016/j.sna.2017.10.013
- 1163 Sørensen, S.P.L. (1909). Enzymstudien II: Über die Messung und die Bedeutung der
 1164 Wasserstoffionenkonzentration bei enzymatischen Prozessen. *Biochemie Zeitung*, 21, 131-200.
 1165 <https://d-nb.info/1125891521/34>
- 1166 Spijkman, M., Myny, K., Smits, E.C.P., Heremans, P., Blom, P.W.M., & de Leeuw, D.M. (2011a) Dual-
 1167 Gate Thin-Film Transistors, Integrated Circuits and Sensors. *Advanced Materials*, 23(29), 3231-
 1168 3242. doi: 10.1002/adma.201101493
- 1169 Spijkman, M., Smits, E., Cillessen, J.F.M., Biscarini, F., Blom, P.W.M., & de Leeuw, D.M. (2011b).
 1170 Beyond the Nernst-limit with dual-gate ZnO ion-sensitive field-effect transistors. *Applied Physics*
 1171 *Letters*, 98(4), 043502-043502-3. doi: 10.1063/1.3546169
- 1172 Staudinger, C., Strobl, M., Breininger, J., Klimant, I., & Borisov, S.M. (2019). Fast and stable optical
 1173 pH sensor materials for oceanographic applications. *Sensors and Actuators B: Chemical*, 282,
 1174 204-217. doi: 10.1016/j.snb.2018.11.048
- 1175 Staudinger, C., Strobl, M., Fischer, J.P., Thar, R., Mayr, T., Aigner, D., Müller, B.J., Müller, B., Lehner,
 1176 P., Mistlberger, G., Fritzsche, E., Ehgartner, J., Zach, P.W., Clarke, J.S., Geißler, F., Mutzberg, A.,
 1177 Müller, J.D., Achterberg, E.P., Borisov, S.M., & Klimant, I. (2018). A versatile optode system for
 1178 oxygen, carbon dioxide, and pH measurements in seawater with integrated battery and logger.
 1179 *Limnology and Oceanography: Methods*, 16(7), 459–473. doi: 10.1002/lom3.10260
- 1180 Stow, C.A., Jolliff, J., McGillicuddy Jr., D.J., Doney, S.C., Allen, J.I., Friedrichs, M.A.M., Rose, K.A., &
 1181 Wallhead, P. (2009). Skill assessment for coupled biological/physical models of marine systems.
 1182 *Journal of Marine Systems*, 76(1-2), 4–15. doi: 10.1016/j.jmarsys.2008.03.011

- 1183 Su, W., Xu, J., & Ding, X. (2016). An Electrochemical pH Sensor Based on the Amino-Functionalized
1184 Graphene and Polyaniline Composite Film. *IEEE Transactions on Nanobioscience*, 15, 8. doi:
1185 10.1109/TNB.2016.2625842
- 1186 Sulka, G.D., Hnida, K., & Brzózka, A. (2013). pH sensors based on polypyrrole nanowire arrays.
1187 *Electrochimica Acta*, 104, 536– 541. doi: 10.1016/j.electacta.2012.12.064
- 1188 Tagliapietra, D., Sigovini, M., Magni, P. (2012). Saprobity: A unified view of benthic succession
1189 models for coastal lagoons. *Hydrobiologia*, 686, 15–28. doi: 10.1007/s10750-012-1001-8
- 1190 Takechi, K., Iwamatsu, S., Konno, S., Yahagi, T., Abe, Y., Katoh, M., & Tanabe, H. (2015). Gate-to-
1191 source voltage response in high-sensitivity amorphous InGaZnO₄ thin-film transistor pH sensors.
1192 *Japanese Journal of Applied Physics*, 54(7), 078004. doi: 10.7567/jjap.54.078004
- 1193 Tan, X., Chuang, H.-J., Lin, M.-W., Zhou, Z., & Cheng, M. M.-C. (2013). Edge Effects on the pH
1194 Response of Graphene Nanoribbon Field Effect Transistors. *Journal of Physical Chemistry C*,
1195 117(51), 27155–27160. doi: 10.1021/jp409116r
- 1196 Tasis, D., Tagmatarchis, N., Bianco, A., & Prato, M. (2006). Chemistry of carbon nanotubes. *Chemical*
1197 *Reviews*, 106(3), 1105-1136. doi: 10.1021/cr050569o
- 1198 Trasatti, S. (1991). Physical electrochemistry of ceramic oxides. *Electrochimica Acta*, 36, 225–241.
1199 doi: 10.1016/0013-4686(91)85244-2
- 1200 Tsai, Y.-T., Chang, S.-J., Ji, L.-W., Hsiao, Y.-J., & Tang, I.-T. (2019). Fast Detection and Flexible
1201 Microfluidic pH Sensors Based on Al-Doped ZnO Nanosheets with a Novel Morphology. *ACS*
1202 *Omega*, 4(22), 19847-19855. doi: 10.1021/acsomega.9b02778
- 1203 Uria, N., Abramova, N., Bratov, A., Muñoz-Pascual, F.-X., & Baldrich, E. (2016). Miniaturized metal
1204 oxide pH sensors for bacteria detection. *Talanta*, 147, 364–369. doi: 10.1016/j.talanta.2015.10.011
- 1205 Weldborg, M., Turner, D.R., Anderson, L.G., & Dyrssen, D. (2009). Determination of pH. In K.
1206 Grasshoff, K. Kremling, & M.Ehrhardt (Eds.), *Methods of Seawater Analysis*, John Wiley & Sons.
- 1207 Wu, Y.-C., Wu, S.-J., & Lin, C.-H. (2017). Mass-produced polyethylene-terephthalate film coated with
1208 tantalum pentoxide for pH measurement under ISFET detection configuration. *Microsystem*
1209 *Technologies*, 23(2), 293-298. doi: 10.1007/s00542-015-2474-y
- 1210 Xu, K., Zhang, X., Hou, K., Geng, M., & Zhao, L. (2016). The effects of antimony thin film thickness on
1211 antimony pH electrode coated with nafion membrane. *Journal of the Electrochemical Society*,
1212 163(8), B417-B421. doi: 10.1149/2.0191608jes
- 1213 Xu, K., Zhang, X., Chen, C., & Geng, M. (2018). Development and Performance of an All-Solid-States
1214 pH Sensor Based on Modified Membranes. *International Journal of Electrochemical Science*, 13,
1215 3080-3090. doi: 10.20964/2018.03.04
- 1216 Yao, S., Wang, M., & Madou, M. (2001). A pH Electrode Based on Melt-Oxidized Iridium Oxide.
1217 *Journal of the Electrochemical Society*, 148(4), H29-H36. doi: 10.1149/1.1353582

- 1218 Yoon, J.H., Hong, S.B., Yun, S.-O., Lee, S.J., Lee, T.J., Lee, K.G., Choi, B.G. (2017). High
1219 performance flexible pH sensor based on polyaniline nanopillar array electrode. *Journal of Colloid*
1220 *and Interface Science*, 490, 53–58. doi: 10.1016/j.jcis.2016.11.033
- 1221 Young, S.-J., & Tang, W.-L. (2019). Wireless Zinc Oxide Based pH Sensor System. *Journal of the*
1222 *Electrochemical Society*, 166(9), B3047-B3050. doi: 10.1149/2.0071909jes
- 1223 Zea, M., Moya, A., Fritsch, M., Ramon, E., Villa, R., & Gabriel, G. (2019). Enhanced Performance
1224 Stability of Iridium Oxide-Based pH Sensors Fabricated on Rough Inkjet-Printed Platinum. *ACS*
1225 *Applied Materials and Interfaces*, 11(16), 15160-15169. doi: 10.1021/acsami.9b03085
- 1226 Zhang, X., Ye, Y., Kan, Y., Huang, Y., Jia, J., Zhao, Y.Chen, C.-T.A., Qin, H. (2017). A new
1227 electroplated Ir/Ir(OH)_x pH electrode and its application in the coastal areas of Newport Harbor,
1228 California. *Acta Oceanologica Sinica*, 36(5), 99–104. doi: 10.1007/s13131-017-1064-5
- 1229 Zhang, W.-D., & Xu, B. (2009). A solid-state pH sensor based on WO₃-modified vertically aligned
1230 multiwalled carbon nanotubes. *Electrochemistry Communications*, 11, 1038–1041. doi:
1231 10.1016/j.elecom.2009.03.006
- 1232 Zhao, R., Xu, M., Wang, J., & Chen, G. (2010). A pH sensor based on the TiO₂ nanotube array
1233 modified Ti electrode. *Electrochimica Acta*, 55(20), 5647-5651. doi:
1234 10.1016/j.electacta.2010.04.102
- 1235 Zhu, Y., Wang, C., Petrone, N., Yu, J., Nuckolls, C., Hone, J., & Lin, Q. (2015). A solid-gated
1236 graphene FET sensor for pH measurements. In *Proceedings of the IEEE International Conference*
1237 *on Micro Electro Mechanical Systems (MEMS)*. doi: 10.1109/MEMSYS.2015.7051097
- 1238 Zuaznabar-Gardona, J.C., & Frago, A. (2018). A wide-range solid state potentiometric pH sensor
1239 based on poly-dopamine coated carbon nano-onion electrodes. *Sensors and Actuators B:*
1240 *Chemical*, 273, 664-671. doi: 10.1016/j.snb.2018.06.103